Computer Networks 248 (2024) 110503

Contents lists available at ScienceDirect

Computer Networks

journal homepage: www.elsevier.com/locate/comnet

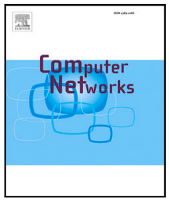

Understanding the impact of persistence and propagation on the Age of Information of broadcast traffic in 5G NR-V2X sidelink communications

Alexey Rolich [a], Ion Turcanu [b,*], Alexey Vinel [c], Andrea Baiocchi [a]

[a] Department of Information Engineering, Electronics and Telecommunications(DIET), University of Rome Sapienza, Italy
[b] Luxembourg Institute of Science and Technology(LIST), Luxembourg
[c] Karlsruhe Institute of Technology(KIT), Karlsruhe, Germany

ARTICLE INFO

Keywords:
5G NR-V2X
Sidelink communications
Age of information
Semi-persistent scheduling
V2X communications
Autonomous resource selection

ABSTRACT

The current Cellular V2X (C-V2X) standard for direct communication between vehicles is based on the so called Semi-Persistent Scheduling (SPS) algorithm. It is based on the multiple access structure of 5G New Radio (NR) and exploits sensing and persistence to realize a randomized multiple access. We consider the application of SPS to support periodic broadcast traffic where no acknowledgments are provided. Persistence is a key feature, which consists of a node using the same resource for its transmissions for multiple frames. The specific resource used is randomly selected from among those that are perceived to be idle, and reselected anew after a randomized number of frames. We define a model to gain insight into the interplay between persistence and key performance metrics for the type of traffic considered, namely probability of successful delivery and Age of Information (AoI). A core version of the model is validated against simulations and used to show that there exists an optimal level that minimizes AoI. The model is then extended to account for a distance-dependent propagation model, allowing further insight into the effects of the interplay between sender–receiver distance and persistence. Finally, an even more detailed model is investigated, using ns-3-based simulations. This further analysis confirms the qualitative behaviors revealed by the analytical model and provides more insight into the complex interactions of system parameters and channel characteristics. The obtained results help to identify the limits of SPS, opening the way to system-principled parameter optimization and design of more powerful variants of the multiple access scheme.

1. Introduction

Connected and automated vehicles are becoming a reality, with several pilots and deployment initiatives underway worldwide [1,2]. V2X communication is a key enabling technology for achieving these initiatives. It enables vehicles and other road users to exchange real-time data with each other and with the road infrastructure to enhance their perception of the environment with non-line-of-sight information.

In order to achieve Vision Zero, which aims for accident free traffic, V2X is expected to support various Cooperative Intelligent Transport Systems (C-ITS) services [3]. From a functional perspective, previous V2X designs have primarily focused on Day 1 services, which include *cooperative awareness* applications [4], such as emergency electronic brake lights and road work warnings. Current standardization efforts aim to support more advanced services, ranging from *collective perception* (Day 2) [5,6], which includes cooperative collision risk warning and lane change assistance, to *coordinated maneuvering* (Day 3) [7] use cases, such as platooning and maneuver coordination at intersections.

While these services may target different levels of functionality, the fundamental enabling communication paradigm is the real-time, periodic exchange of time-sensitive sensor information. For this purpose, two main families of V2X standards have been proposed and developed [8]: Vehicular Wi-Fi (IEEE 802.11p/bd), which includes DSRC/ WAVE in the US [9] and ETSI ITS-G5 in the EU [10], and C-V2X, which includes LTE-V2X [11] and 5G NR-V2X [12]. Between these two families, C-V2X is seeing a higher adoption rate, with the US, China, and South Korea already opting in its favor, while the EU is technology neutral for the time being.

To support the low-latency requirements of V2X applications, C-V2X introduces sidelink communication, which enables direct communication between vehicles without the involvement of a base station. Sidelink resources can be allocated in a centralized manner (i.e., resources are scheduled by the base station) under Mode 3 in LTE-V2X and Mode 1 in 5G NR-V2X, or in a distributed manner (i.e., vehicles autonomously select their resources) under Mode 4 in LTE-V2X and Mode

* Corresponding author.
E-mail addresses: alexey.rolich@uniroma1.it (A. Rolich), ion.turcanu@list.lu (I. Turcanu), alexey.vinel@kit.edu (A. Vinel), andrea.baiocchi@uniroma1.it (A. Baiocchi).

https://doi.org/10.1016/j.comnet.2024.110503
Received 15 January 2024; Received in revised form 6 May 2024; Accepted 9 May 2024
Available online 13 May 2024

2 in 5G NR-V2X. The C-V2X autonomous sidelink resource scheduling mechanism is known as SPS. Under SPS, each user can randomly select a transmission opportunity from a pool of available resources each time there is an update message to transmit. Alternatively, the user can keep the selected channel resource for a certain time window before randomly switching to another one. In the latter case, the persistence probability characterizes the frequency of such a switch. In both cases, users may unfortunately choose the same resource, resulting in mutual interference and preventing others from receiving updates. This work addresses the key research question of whether this persistence is beneficial for performance, which is not intuitively clear in this context. Persistence can be viewed as a form of reservation in a random access scheme, according to classical multiple access theory [13].

1.1. AoI in V2X

In recent years, the performance evaluation of status broadcast updates in V2X has been characterized not only by traditional communication network metrics such as throughput, packet delivery ratio, or mean delay. Instead, similar to other machine-to-machine communication systems, where the freshness of the update information is crucial, AoI is proposed [14,15]. In general, AoI is an end-to-end metric that assesses the timeliness of status update information from an application perspective. AoI performance is affected not only by the various packet delays, including channel access, transmission, propagation, and processing, but also by the loss of packets (e.g., due to collisions, path loss) that carry status updates.

In the context of cooperative awareness and collective perception, AoI is the key performance metric that characterizes a vehicle's environmental sensing gains due to V2X communication [16]. For cooperative maneuvering, AoI can be used in the formal safety evaluation of automated driving [17]. Given its importance for V2X safety applications, understanding the various elements and implications that can affect the AoI performance is critical.

1.2. Our contribution

The random resource selection mechanism in SPS is known to be prone to packet collisions, which directly affects the AoI metric and hinders the efficiency of V2X safety applications. An important parameter in the SPS configuration that can influence the collision loss rate is the persistence probability P. Despite this obvious link, there is very little research in the literature that investigates the impact of the persistence probability on the AoI metric.

In a preliminary work [18], we investigated the interplay between persistence probability and AoI in C-V2X sidelink communication. In particular, we proposed a mathematical model to characterize the performance of the SPS in 5G NR-V2X from the perspective of AoI. The model is based on the assumption that messages transmitted without collision are always decoded, while messages subject to collisions are always lost.

The current paper is an extended version of our preliminary paper [18], which includes additional enhancements to the previously proposed model. Specifically, it relaxes the previous assumption and allows for a classic propagation model that considers both a distance-based deterministic component and a stochastic component that accounts for fading. Additionally, this extended version evaluates the performance of the proposed model using a detailed system-level network simulator.

The contributions of this paper can be summarized as follows:

- An analytical model is developed to examine the relationship between persistence probability and AoI in 5G NR-V2X sidelink communications.
- The model is validated through MATLAB-based simulations, which demonstrate that the AoI is non-monotonic in relation to the persistence probability. An optimal level that minimizes the AoI's value can be found.
- We propose an extension of the core model to capture the effect of distance-based propagation and fading.
- The proposed model is further evaluated using detailed ns-3 based simulations, which confirm the qualitative behavior revealed by the analytical model.

Table 1
List of acronyms.

Acronym	Meaning
AoI	Age of Information
ANRM	All-or-Nothing Receiver Model
BSM	Basic Safety Message
CAM	Cooperative Awareness Message
CBR	Channel Busy Ratio
C-ITS	Cooperative Intelligent Transport Systems
C-V2X	Cellular V2X
DDPM	Distance-Dependent Propagation Model
DS	Dynamic Scheduling
DSRC	Dedicated Short-Range Communication
DTMC	Discrete Time Markov Chain
ETSI	European Telecommunications Standards Institute
ITS	Intelligent Transportation Systems
LTE	Long-Term Evolution
NR	New Radio
PAoI	Peak AoI
PCR	Packet Collision Ratio
PDF	Probability Density Function
PDR	Packet Delivery Ratio
PIR	Packet Inter-Reception Delay
PRR	Packet Reception Ratio
RB	Resource Block
RC	Reselection Counter
RRI	Resource Reservation Interval
RSRP	Reference Signal Receive Power
SC	Sub-Channel
SCI	Sidelink Control Information
SPS	Semi-Persistent Scheduling
TB	Transport Block
UE	User Equipment
V2X	Vehicle-to-Everything
WAVE	Wireless Access in Vehicular Environments

The rest of the paper is organized as follows. Section 2 provides an overview of NR-V2X sidelink communications and analyzes related works on the performance evaluation of SPS and AoI metric. Section 3 describes the proposed analytical model. Section 4 validates the analytical model through simulations and presents the obtained results. Section 5 evaluates the model in a highway environment using a system-level simulator. Section 6 concludes the paper. Table 1 presents the acronyms utilized in this paper.

2. Background and related work

5G NR-V2X sidelink technology has recently been introduced to enable advanced use cases that rely on cooperative perception and maneuvering [19]. Comprehensive overviews of 5G NR-V2X, describing its physical layer design and resource allocation mechanisms, as well as its two operation modes (Mode 1 and Mode 2), are provided in [20–23]. While Mode 1 relies on a centralized resource allocation mechanism, Mode 2 introduces two distributed allocation strategies – SPS and Dynamic Scheduling (DS) – that allow vehicles to select their transmission resources autonomously.

In this section, we first provide an overview of the resource allocation mechanism in NR-V2X Mode 2. We then analyze the related works that investigate the performance of the SPS mechanism in terms of the most common metrics. We finally describe the existing literature that analyzes the AoI metric in the context of 5G NR-V2X.

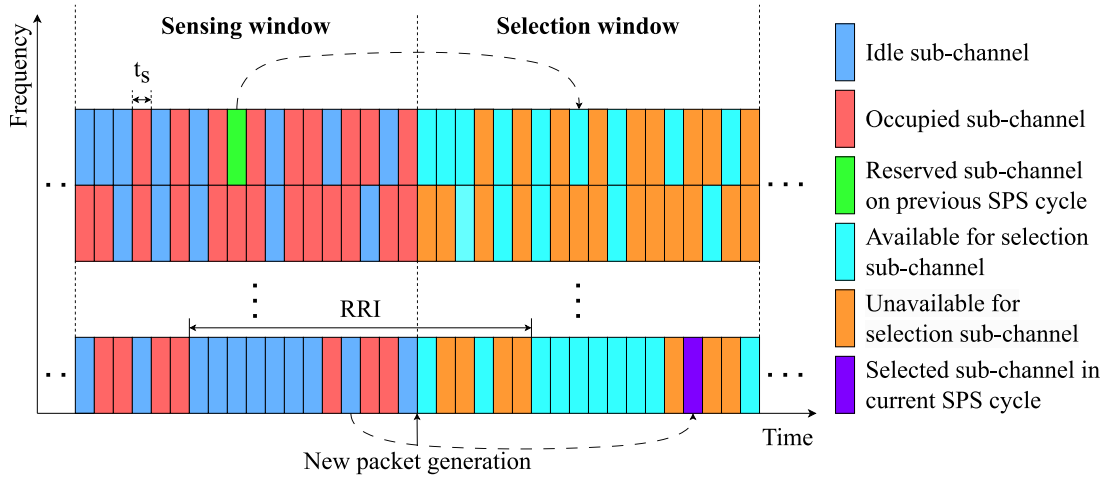

Fig. 1. Simplified example of SPS-based scheduling in NR-V2X Mode 2.

2.1. Overview of NR -V2X Mode 2

In NR-V2X, messages are transmitted in Transport Blocks (TBs). The communication resources allocated to TBs are called Sub-Channels (SCs). An SC consists of several Resource Blocks (RBs) belonging to the same time slot and occupying adjacent frequencies. An SC carries a control field called Sidelink Control Information (SCI) and a TB or part of a TB, if the latter is fragmented across multiple SCs.

There are two possible approaches to allocate resources for TB transmission in Mode 2 - DS and SPS [24]. In DS mode, resources are selected each time a new TB is generated. SPS, instead, selects resources and keeps them for a number of consecutive RC TBs.

The time period between consecutive TB transmissions is determined by the Resource Reservation Interval (RRI). Possible RRI values are {0, [1: 99], 100, 200, 300, 400, 500, 600, 700, 800, 900, 1000} ms. The RRI is selected for every new TB from a list of maximum 16 pre-configured values in the resource pool [25].

The RC value depends on the selected RRI and is randomly chosen every time a new resource must be selected. In particular, RC is randomly chosen within $[5, 15]$ when $RRI \geq 100\,\text{ms}$. If $RRI < 100\,\text{ms}$, then RC is randomly set within $[5 \cdot C, 15 \cdot C]$, where

$$C = \frac{100}{\max(20, RRI)}. \tag{1}$$

RC is decremented by 1 with every TB transmission. When RC = 0, a new resource is selected with probability $(1 - P)$, where $P \in [0, 0.8]$. Otherwise, the same resources with the same RRI will be used for a number of consecutive RC TBs, where RC is again randomly chosen according the rules described above.

A simplified example of the SPS resource selection process is shown in Fig. 1. Each User Equipment (UE) has a *sensing window* (of 1100 ms or 100 ms, depending on the configuration), used to determine which SCs are reserved by other UEs for their own TB transmissions. If the RSRP of these transmissions exceeds a preconfigured threshold, they are excluded from the pool of candidate resources in the *selection window*. In particular, the SPS resource selection algorithm has two main steps [20]:

1. Exclude candidate resources (i.e., SCs) in the selection window corresponding to (i) reservations received from other UEs in the 1st-stage SCI detected during the sensing window; (ii) measurements of a received power level exceeding a given threshold for those SCs for which no explicit reservation could be verified. Other SCs are also excluded, corresponding to those that cannot be received and checked by the node during the sensing window due to half-duplex operations.
2. Randomly select the sidelink resource from the list of available candidate resources.

2.2. Related works on SPS Performance Evaluation

2.2.1. LTE-V2X Mode 4

Several recent works have investigated the performance of cellular V2X sidelink communication. Gonzalez-Martín et al. [26] developed analytical models to evaluate the performance of LTE-V2X Mode 4 [27], focusing on the PDR and different types of packet errors. Segata et al. [28] analyzed the impact of LTE-V2X Mode 4 on vehicle platooning, noting significant limitations due to packet loss even in low traffic conditions.

Further research in [29] examines how the persistence probability affects PDR, finding that higher probabilities do not necessarily improve PDR. Another study [30] discusses delay performance optimization in SPS, suggesting optimizations of several configuration parameters, such as sensing range, transmit power, and resource reservation.

Bazzi et al. [31] propose enhancing the SPS mechanism to address packet losses due to incorrect resource allocation in LTE-V2X Mode 4, showing that their extended mechanism outperforms the legacy SPS in terms of Packet Reception Ratio (PRR). Wu et al. [32] suggest replacing SPS with a self-adaptive scheduling protocol to address the half-duplex and packet collision issues, demonstrating better PDR and throughput.

The coexistence of periodic and aperiodic traffic in LTE-V2X Mode 4 is investigated in [33], where a new standard-compliant resource reservation mechanism to handle aperiodic traffic is proposed and an analytical model for the throughput is defined. Bartoletti et al. [34] analyze the impact of the mismatch between the packet generation and resource allocation on the system performance, revealing potential performance boosts by reserving resources more frequently. Jeon et al. [35] show that message collisions in LTE-V2X Mode 4 can be reduced by reducing the uncertainties in the resources to be used for the next sequence of messages, though at the cost of higher overhead. Haider and Hwang [36] advocate for power control in CAM transmissions to enhance LTE-V2X Mode 4 performance, particularly beneficial in high-density scenarios.

2.2.2. 5G NR-V2X Mode 2

Todisco et al. [36] and Molina-Galan et al. [37] focused on optimizing NR-V2X Mode 2 for periodic and aperiodic traffic respectively, emphasizing the need for tailored resource allocation strategies and improvements to the MAC layer for better traffic management. Cao et al. [38] explored resource scheduling for vehicular platooning in 5G NR-V2X, proposing an enhanced random selection scheme that effectively reduces collision probabilities. The performance of SPS in the use case of cooperative perception is investigated in [6] using a realistic system-level network simulator.

A comparative analysis of the SPS and DS mechanisms in 5G NR-V2X Mode 2 is performed in [39] and an adaptive scheduling strategy that allows dynamic selection of the most appropriate scheme in the presence of mixed traffic types is proposed. In [40], the authors propose to integrate resource reuse distance judgment with SPS to mitigate conflicts and interference during resource selection, demonstrating higher PRR and reduced inter-packet gap in various scenarios compared to conventional schemes.

Lusvarghi et al. [41] propose a machine learning based approach to predict CAM sequences in order to adapt the RRI to minimize packet collisions. Kuang et al. [42] use adaptive RC and RRI adjustment to accommodate aperiodic traffic, minimizing collision effects and demonstrating improved communication quality and resource utilization efficiency through theoretical modeling and simulations.

Recent studies advocate for the use of Non-Orthogonal Multiple Access (NOMA) for 6G-V2X and demonstrate its potential through simulations [43,44]. Twardokus et al. [45] identify vulnerabilities in the physical layer attributes and the SPS algorithm, implementing two denial-of-service attacks, as well as machine learning-based mitigation techniques to enhance the security of 5G V2X.

2.3. Related works on AoI in 5G NR-V2X

The studies described in Section 2.2 provide valuable insight into the performance of SPS. However, none of these works analyze the AoI [14], which is a critical performance metric that measures the freshness of cooperative awareness and perception message updates. Although it has been extensively studied in the context of IEEE 802.11-based vehicular communications [16,46–48], there are only few existing works that analyze the AoI performance in 5G NR-V2X.

Peng et al. [49] pioneered AoI optimization in cellular sidelink communications, proposing a resource allocation mechanism with piggyback feedback to reduce collisions, though it struggles with aperiodic traffic. Another study [50] introduces an adaptive SPS enabling real-time RRI adjustments, enhancing traffic safety and network performance through an AoI-aware algorithm that selects optimal RRIs based on neighboring vehicles' AoI, significantly improving cooperative awareness in NR-V2X scenarios.

Fouda et al. [51] explore reducing the probability of persistent Basic Safety Message (BSM) collisions by randomly skipping SPS reserved resources, merging one-shot transmissions with SPS to enhance AoI. Saad et al. [52] utilize deep reinforcement learning for congestion control in 5G NR-V2X. Unlike traditional decentralized algorithms, the proposed solution optimizes the Medium Access Control (MAC) layer by considering both system-level metrics and application-level requirements such as AoI. The proposed scheme outperforms the standard 3GPP decentralized congestion control, showing superior results in packet delivery, message timeliness, throughput, and channel occupancy.

Cao et al. [53] analyze SPS parameters from an AoI perspective, revealing that RRI greatly influences the PAoI. However, the AoI metric is not considered as a possible parameter of the SPS mechanism. The impact of the radio resource keeping probability on AoI is also not investigated. The authors conclude that the number of successful transmissions is not sensitive to changes in radio resource persistence probability.

The authors in [54] propose to minimize the AoI in 5G NR-V2X Mode 1 (centralized) using NOMA in half-duplex settings. In particular, they formulate the AoI minimization problem as a mixed-integer nonlinear program and prove its NP-hardness. They model the problem as a single-agent Markov decision process and use a deep reinforcement learning approach to find the transmission power levels and broadcast coverage areas.

In our previous work [18], we investigated the impact of persistence on AoI in 5G NR-V2X Mode 2. We defined a simplified analytical model of the SPS that allows easy evaluation and optimization of the persistence probability P, i.e., the probability of keeping the same resources for the next packet transmissions, from an AoI perspective. The current work is an extension of our previous study that further improves the previously proposed model to account for the propagation loss. By means of system-level simulations, we also obtain a qualitative confirmation of the results previously obtained in [18], which suggest the existence of an optimal persistence level.

3. System model

This section introduces a model of SPS using an ANRM. The model provides insight into the role of persistence in SPS, although it is quite simplified. In the final part of this section, a more realistic propagation model is defined, and the preceding analysis is extended.

3.1. Model assumptions and notation

Consider a set of N nodes that share a 5G NR-V2X communication channel used according to Mode 2 [53]. The question we aim to answer is whether persistence is beneficial for cooperative awareness and to what extent. To fully understand this point, we use a simplified model that retains the essential characteristics of the SPS contention algorithm. We make the following assumptions:

1. *All-or-Nothing Receiver Model*: messages transmitted without collision (i.e., only one message is transmitted in the used SC) are always correctly decoded; messages undergoing collisions (i.e., multiple messages are transmitted in the same SC) are always lost.
2. All nodes hear each other (no hidden nodes).
3. All nodes use the same RRI.
4. The sensing window used by a node to identify candidate SCs extends over exactly one RRI.
5. Only broadcast traffic is considered, i.e., no ACK is provided and no retransmission is scheduled.
6. Nodes generate a new message in each RRI.
7. The SC is sized to carry one complete message, i.e., one TB plus its associated SCI (both first and second stage).
8. The RC is drawn from a Geometric probability distribution, i.e., $\mathcal{P}(RC = j) = c^{j-1}(1-c)$, for $j \geq 1$. Note that the mean RC is equal to $\overline{RC} = 1/(1-c) \geq 1$, hence c can be identified as $c = 1 - 1/\overline{RC}$.
9. The number of nodes N is less than the number K of SCs available in one RRI.

Assumption 1 does not account for the so called Wireless Blind Spot (WBS) issue [31]. While transmitting on a given SC j, it is not possible for a node to hear anything transmitted in *another* SC belonging to the same time slot as SC j. It is also not possible to make reliable sensing. This simplification has a minor impact in practical settings, where there are few SCs in the same slot (e.g., less than 4 or 5) and hundreds of SCs within an RRI time. In general, the proposed model is oblivious of the detailed time–frequency organization of radio resources, which simplifies notation, while entailing negligible loss of accuracy, given the marginal effect of WBS. Assumptions 6 and 7 correspond to the best situation for the SPS algorithm, since message generation is exactly periodic and each new message fits exactly into the reserved resource. It is known that SPS can lead to wasted resources and inefficiency in case of non-periodic message generation times and variable message sizes [53]. In this analysis, we assume the best possible configuration for SPS, since our goal is to understand the impact of persistence on performance and to optimize system configuration in a context where the persistent approach of this algorithm makes sense. Note also that, as a consequence of Assumption 9, there is always at least one idle SC in each RRI. Assumption 4 is actually implied by the fact that nodes generate new messages periodically, provided that the selection window is not smaller than the common value of the RRI of all nodes.

Table 2
Main notation used in the paper.

Symbol	Meaning
N	Number of nodes.
K	Number of SCs per RRI.
P	Persistence probability, i.e., the probability that a node keeps its current SC once its RC counter expires.
c	Parameter of the Geometric distribution of the RC; it is $\overline{RC} = 1/(1-c)$, where $\overline{RC}$ denotes the mean RC value.
q	Probability to change the SC in the next RRI with respect to the currently used one. It is $q = (1-P)(1-c)$.
$X_i(t)$	State of SC i in the tth RRI, defined as the number of nodes that are currently using SC i to transmit their messages; it is $X_i(t) \in \{0, 1, \dots, N\} (i = 1, \dots, K)$.
$S_j(t)$	State of node j in the tth RRI, defined as 1 if node j transmits its message with success in that RRI, 0 otherwise $(j = 1, \dots, N)$.
Y	Number of RRIs elapsing between two successfully delivered messages originating from a same node.

Let K be the number of SCs available in the selection window, i.e., in one RRI. In each RRI, each node uses one SC to broadcast its message. If more than one node uses the same SC, we assume that mixed signals cannot be separated and recovered by other nodes and thus the collision turns into a loss of the messages involved.

A node selects an idle SC[1] and persists using it for a number of times equal to its value of RC. Once RC is counted down to 0, the node decides to draw a new value of RC and persist on the same SC with probability P. With probability $1 - P$, the node switches to another idle SC and draws a new value of RC.

The selection of a new SC (SC re-selection procedure) is based on the measurements collected in the sensing window. There is no point in including SCs that are sensed as busy in the candidate SC list, since a collision would certainly be triggered. Therefore, we assume that a node that decides to jump to a new SC in a given RRI selects the target SC *uniformly at random among all those SCs that were idle in the previous RRI*. On those measurements, a node constructs a table of available SCs in a forthcoming re-selection window. The table is used to pick the new SC. We simplify this process by identifying the selection window with one RRI and assuming perfect sensing. Under these assumptions, since there are no hidden nodes, each node classifies SCs as either in use or idle, the latter state being identified only if no node is using that SC.

The main notation used in the paper is listed in Table 2.

3.2. Model analysis

Let us take the point of view of one SC, referred to as the *tagged SC*. This is possible because the modeling assumptions imply full symmetry of resource use, so that all SCs are statistically equivalent. Let us define the state $X \in \{0, 1, \dots, N\}$ associated with the tagged SC, as the number of nodes currently using the tagged SC for their transmission. If $X = 0$, the SC is idle and available for re-selection. If $X = 1$, only a single node is using the SC, so its transmission will not collide with others and the relevant message will be decoded successfully by all other nodes. If $X > 1$, multiple nodes are using the same SC for their transmissions. Then, a collision occurs and no involved message can be decoded correctly by any node.

Let $X_i(t)$ be the state of SC i at time t, with $i = 1, \dots, K$ and $t \geq 0$. Let us distinguish two cases.

First, if $X_i(t) > 0$, the ith SC is currently used by at least one node. Thanks to sensing, no other node will attempt to jump to SC i. However, a node currently using this SC can decide to switch to another SC, if its RC has expired and the node does not persist using that same SC. A node switches to another SC with probability

$$q = (1-c)(1-P) = \frac{1-P}{\overline{RC}}, \tag{2}$$

where $\overline{RC}$ is the average of the initial value of the RC. Given the argument above, any state $X_i(t) > 0$ can only decrease as t increases, eventually hitting the state 0.

The second case is when $X_i(t) = 0$. Then, SC i can be selected by nodes jumping from their current SC $j \neq i$, which causes the state $X_i(t+1)$ to become positive, in case at least one node performs a re-selection procedure towards SC i.

Let us define the N-dimensional stochastic process $\mathbf{X}(t) = [X_1(t), \dots, X_K(t)]$, living on the state space $\mathcal{S} = \{0, 1, \dots, N\}^K$. Thanks to the memoryless assumption on the SC re-selection process, $\mathbf{X}(t)$ is a Discrete Time Markov Chain (DTMC). In view of the model assumptions, it follows that $\mathbf{X}(t)$ is time-homogeneous, irreducible, aperiodic and has a finite state space, hence it is ergodic and a unique limiting stationary probability distribution exists for the steady state process $\mathbf{X}(\infty)$. In the following, the argument ∞ will be dropped when referring to the steady-state process, if there is no ambiguity.

Let the transition probability of $X_i(t)$, conditional on the state at time t be defined as

$$P_i(n,k) = \mathcal{P}(X_i(t+1) = k | X_i(t) = n, \mathbf{X}_{-i}(t) = \mathbf{x}_{-i}) \tag{3}$$

where $\mathbf{X}_{-i}(t)$ is a row vector containing all SC states $X_j(t)$ with $j \neq i$ and $\mathbf{x}_{-i}$ is a row vector of $N-1$ entries, each entry belonging in the set $\{0, 1, \dots, N\}$, with the constraint that $\sum_{j \neq i} x_{-i}(j) + n = N$.

The conditional state transition probabilities of SC i can be written as follows:

$$\begin{cases} P_i(n,k) = \binom{n}{k}(1-q)^k q^{n-k} & \text{for } n > 0, 0 \leq k \leq n, \\ P_i(n,k) = 0 & \text{for } n > 0, k > n \\ P_i(0,k) = \binom{N}{k} w^k (1-w)^{N-k} & \text{for } n = 0, 0 \leq k \leq N, \end{cases} \tag{4}$$

where

$$\begin{cases} w = \frac{q}{K_e(i)} \\ K_e(i) = \sum_{j=1}^{K} I(X_j(t) = 0) \end{cases} \tag{5}$$

and $I(E)$ is the indicator function of the event E. The quantity $K_e(i)$ is therefore the number of idle SCs.

The first two equations tell us that the number of nodes using the same SC simultaneously cannot grow, thanks to channel sensing. The third equation takes into account that new nodes choose SC i when they switch from their current SC (different from i).

The SC states $X_i(t)$, $i = 1, \dots, K$, are coupled together, since the number of SCs that are idle, $K_e(i)$, is a function of the state of all SCs other than the tagged one, namely SC i. We should therefore consider the entire K-dimensional DTMC $\mathbf{X}(t) = [X_i(t), X_2(t), \dots, X_K(t)]$, with state space size of $(N+1)^K$.

To tame the complexity of this formidable DTMC, we use a mean field approximation, which is obtained by replacing $I(X_j(t) = 0)$ with its mean, i.e., with the probability that SC j is empty, $\pi_{0,j}$. Thus, we effectively replace $K_e(i)$ (which is generally a random variable) with its mean $\overline{K}_e(i)$, namely, the mean number of idle SCs in one RRI. Note that $0 < \overline{K}_e(i) < K$. In fact, $K_e(i)$ cannot reduce to 0 due to our assumption that $N < K$. On the other end, $K_e(i) = K$ is not possible as well, since the N nodes must be occupying at least one SC.

Quantities related to the mean field approximation are denoted by a tilde, i.e., $\tilde{X}_i(t)$ denotes the number of nodes that use SC i in the tth

[1] According to the SPS algorithm, SCs eligible for selection are those that are found to be idle and those that report an RRI value of 0 in their SCI. This special value of RRI is set by a node that is using an SC for the last time, i.e., a node whose RC has dropped to 0 and that has decided not to persist on its currently used SC. We do not consider this detail, assuming that only SCs detected as idle are available for selection. An exploratory study shows that the results obtained by the model presented here do not change even if this detail is taken into account, i.e., the average AoI is minimized in both cases for a suitable value of the persistence probability.

RRI according to the approximate process obtained with the mean field approximation.

It can be seen that in the considered model setting, SCs are statistically equivalent, as well as nodes, so that the number of nodes transmitting on one SC has the same probability distribution for all SCs, i.e., $\tilde{X}_i(t) \sim \tilde{X}_j(t)$, $\forall i, j$. Hence, the probability distribution of $\tilde{X}_i(t)$ does not depend on the index i. Therefore, denoting the approximate transition probabilities with a tilde and dropping also index i for the sake of simpler notation, we can write

$$\begin{cases} \tilde{P}(n,k) = \binom{n}{k}(1-q)^k q^{n-k} & n > 0, 0 \le k \le n \\ \tilde{P}(n,k) = 0 & n > 0, k > n \\ \tilde{P}(0,k) = \binom{N}{k}\left(\frac{q}{\overline{K}_e}\right)^k \left(1 - \frac{q}{\overline{K}_e}\right)^{N-k} & 0 \le k \le N \end{cases} \tag{6}$$

where $\overline{K}_e$ is the mean number of empty SCs.

The stationary probability vector $\tilde{\boldsymbol{\pi}} = [\tilde{\pi}_0, \dots, \tilde{\pi}_N]$ is found by solving the linear system $\tilde{\boldsymbol{\pi}}\tilde{\mathbf{P}} = \tilde{\boldsymbol{\pi}}$, with the condition $\sum_{k=0}^{N} \tilde{\pi}_k = 1$, where $\tilde{\mathbf{P}}$ is a stochastic matrix whose entries are $\tilde{P}(n,k)$ for $n, k = 0, 1, \dots, N$.

The quantity $\overline{K}_e$ in Eq. (6) can be expressed as follows

$$\overline{K}_e = K\tilde{\pi}_0 \tag{7}$$

From Eqs. (6) and (7) it is clear that the numerical solution of the DTMC $\tilde{X}(t)$ is obtained by means of a fixed-point iteration on the quantity $\tilde{\pi}_0$. For a given value of $\tilde{\pi}_0$, the one-step transition probabilities in Eq. (6) are computed by using Eq. (7), the DTMC stationary vector $\tilde{\boldsymbol{\pi}}$ is found, and a new value of $\tilde{\pi}_0$ is evaluated.

It is possible to exploit the special structure of the one-step transition probability matrix $\tilde{\mathbf{P}}$ to obtain a more explicit form of the fixed point equation.

It is easy to see that $\tilde{\mathbf{P}}$ has the following special structure:

$$\mathbf{P} = \begin{bmatrix} \tilde{P}(0,0) & \mathbf{v} \\ \mathbf{a} & \mathbf{A} \end{bmatrix} \tag{8}$$

where $\mathbf{v} = [\tilde{P}(0,1), \dots, \tilde{P}(0,N)]$ is a row vector of size N, $\mathbf{a} = \mathbf{e} - \mathbf{A}\mathbf{e}$ is a column vector of size N, and $\mathbf{A}$ is a lower triangular matrix of size $N \times N$. Here $\mathbf{e}$ denotes a column vector of 1's of size N. We introduce also the notation $\mathbf{I}$ to denote the identity matrix of size $N \times N$.

Let us split the stationary probability vector $\tilde{\boldsymbol{\pi}}$ as follows: $\tilde{\boldsymbol{\pi}} = [\tilde{\pi}_0, \tilde{\boldsymbol{\pi}}_{-0}]$, where $\tilde{\boldsymbol{\pi}}_{-0} = [\tilde{\pi}_1, \dots, \tilde{\pi}_N]$ is a row vector of size N collecting state probabilities for states $1 \le k \le N$. From $\tilde{\boldsymbol{\pi}}\tilde{\mathbf{P}} = \tilde{\boldsymbol{\pi}}$, using Eq. (8), it can be verified that

$$\tilde{\boldsymbol{\pi}}_{-0} = \tilde{\pi}_0 \mathbf{v}(\mathbf{I} - \mathbf{A})^{-1} \tag{9}$$

Then, from $\tilde{\pi}_0 + \tilde{\boldsymbol{\pi}}_{-0}\mathbf{e} = 1$, we have

$$\tilde{\pi}_0 = \frac{1}{1 + \mathbf{v}(\mathbf{I} - \mathbf{A})^{-1}\mathbf{e}} \tag{10}$$

This is a fixed point equation in $\tilde{\pi}_0$, given that the entries of $\mathbf{v}$ depend on $q/\overline{K}_e$ and hence on $\tilde{\pi}_0$ in view of Eq. (7). This equation is easily handled for N and K in the range of hundreds. For very large values of N, the DTMC could be truncated, exploiting the fast decay of the probability distribution $\tilde{\boldsymbol{\pi}}$.

The numerical solution of Eq. (10) is found by iteration, starting from an initial value $x_0 \in (0,1)$. The following theorem guarantees existence and uniqueness of a solution for $\tilde{\pi}_0$.

Theorem 1. *If $N < K$, a unique solution $\xi \in (0,1)$ exists for Eq. (10) and it belongs to the interior of the interval $[0,1]$. The sequence generated by iterating Eq. (10) is convergent to ξ for any initial value $x_0 \in (0,1)$.*

Proof. The proof is given in Appendix. □

Further, let $\mathbf{u}$ denote a column vector of size N such that $u(k) = k$, $k = 1, \dots, N$. Given the special form of entries of $\mathbf{A}$ (see Eq. (6)), it can be found that $\mathbf{A}\mathbf{u} = (1-q)\mathbf{u}$, i.e., $\mathbf{u}$ is a right eigenvector of $\mathbf{A}$ with eigenvalue $1-q$. For $q < 1$, it follows that

$$\sum_{k=1}^{N} k\tilde{\pi}_k = \tilde{\boldsymbol{\pi}}_{-0}\mathbf{u} = \tilde{\pi}_0 \mathbf{v}(\mathbf{I} - \mathbf{A})^{-1}\mathbf{u} = \tilde{\pi}_0 \mathbf{v}\mathbf{u}\frac{1}{q} \tag{11}$$

Using expressions in Eq. (6), it can be found that $\mathbf{v}\mathbf{u} = Nq/\overline{K}_e$. Hence

$$\sum_{k=1}^{N} k\tilde{\pi}_k = \tilde{\pi}_0 \frac{N}{\overline{K}_e} = \frac{N}{K} \tag{12}$$

where we have exploited Eq. (7) in the last passage. This result has a simple intuitive interpretation. It expresses a conservation law, i.e., K times the mean number of nodes using one SC is just N, the overall number of nodes.

Performance metrics can be evaluated once the probability distribution $\tilde{\boldsymbol{\pi}}$ is found. The average throughput in one RRI is $K\tilde{\pi}_1$, since $\tilde{\pi}_1$ is the probability that a node is the only one using its current SC. The success probability of a node, conditional on the node transmitting, is therefore

$$p_s = K\tilde{\pi}_1/N. \tag{13}$$

3.3. AoI Analysis

The time evolution of a tagged node's message delivery can be tracked using a two-state DTMC $S(t)$, where we drop the subscript denoting the specific node, since nodes are statistically equivalent. We let $S(t) = 1$, if the tagged node's message is transmitted without collision in RRI t, otherwise we have $S(t) = 0$. The transmission of a message is successful if and only if the selected SC is used only by the tagged node (all-or-nothing receiver model).

The two-state Markov chain $S(t)$ captures the semi-persistent nature of the resource allocation. It shows that the semi-persistent scheduling induces a Gilbert-Elliot behavior on the communication channel of the nodes. That is, the flow of messages issued by a node alternates between success states, where each message is correctly received by the neighbors of the transmitting node, and off states, where the messages issued by the tagged node run into a series of collisions (as long as the tagged node persists in using the same SC) and are lost.

Given that $S(t) = 1$, the next message will be successful if: (i) the node does not switch its SC, or (ii) the node switches to a new idle SC and no other node selects that same SC. Hence

$$p_{11} = \mathcal{P}(S(t+1) = 1 \mid S(t) = 1) = 1 - q + q\left(1 - \frac{q}{\overline{K}_1}\right)^{N-1} \tag{14}$$

where $\overline{K}_1$ is the mean number of empty SCs seen in the considered state transition, as detailed below.

Let $SC(t)$ be the SC where the tagged node transmits in RRI t (and is successful, since $S(t) = 1$). The quantity $\overline{K}_1$ is the mean number of idle SCs among the $K-1$ SCs other than the SC used by the tagged node in RRI t. Since the tagged node is in the "success" state, it is the only one using its SC. The other $N-1$ nodes populate the remaining $K-1$ SCs. The mean number of nodes in each busy SC, other than the tagged node's SC, is given by

$$\overline{Q}_{1,N} = \mathrm{E}[X \mid 1 \le X \le N-1] = \frac{\sum_{k=1}^{N-1} k\tilde{\pi}_k}{1 - \tilde{\pi}_0 - \tilde{\pi}_N} \tag{15}$$

Then, we have

$$\overline{K}_1 = K - 1 - \frac{N-1}{\overline{Q}_{1,N}} \tag{16}$$

Using Eq. (12), it can be verified that $\overline{K}_1 \approx K\tilde{\pi}_0$. It turns out that this approximation is within less than 1% relative error in all of our numerical evaluations. This completes the evaluation of p_{11}.

Now we turn to the transition probability

$$p_{00} = \mathcal{P}(S(t+1) = 0 \mid S(t) = 0). \tag{17}$$

This is achieved by requiring that the limiting probability of state 1 coincides with the success probability, namely

$$\mathcal{P}(S(t)=1)=\frac{1-p_{00}}{2-p_{11}-p_{00}}=p_s, \tag{18}$$

where p_s is given in Eq. (13) and p_{11} in Eq. (14).

After obtaining p_{11} and p_{00}, we can calculate the time elapsed between two successful transmissions of a node by evaluating its moments. Let Y represent the corresponding random variable, expressed in units of RRI. Y is an integer greater than or equal to 1 and is defined as the time it takes a node to deliver a new successful message since it delivered the last successful message. Regarding the two-state Markov chain that characterizes the node activity, this means the time to return to state $S=1$ after having just visited state 1. In other words, Y represents the time it takes to reach state 1 for the first time, assuming that the DTMC is initialized in state 1. If V_0 denotes the visit time in state $S=0$, we have

$$Y=\begin{cases}1 & \text{w.p. } p_{11},\\ 1+V_0 & \text{w.p. } p_{10}=1-p_{11}.\end{cases} \tag{19}$$

The random variable V_0 is Geometric with ratio p_{00}, hence

$$\begin{cases}\mathrm{E}[V_0]=\frac{1}{1-p_{00}}\\ \mathrm{E}[V_0^2]=\frac{1+p_{00}}{(1-p_{00})^2}\end{cases} \tag{20}$$

It follows that

$$\begin{cases}\mathrm{E}[Y]=1+\frac{1-p_{11}}{1-p_{00}}=\frac{1}{p_s}\\ \mathrm{E}[Y^2]=1+\frac{(1-p_{11})(3-p_{00})}{(1-p_{00})^2}=\frac{1}{p_s}+\frac{2(1-p_s)^2}{p_s^2(1-p_{11})}\end{cases} \tag{21}$$

By definition, we have the following final result for the average AoI and PAoI metrics (in units of RRI):

$$\begin{cases}\mathrm{E}[\mathrm{PAoI}]=\mathrm{E}[Y]=\frac{1}{p_s}\\ \mathrm{E}[\mathrm{AoI}]=\frac{\mathrm{E}[Y^2]}{2\mathrm{E}[Y]}=\frac{1}{2}+\frac{(1-p_s)^2}{p_s(1-p_{11})}\end{cases} \tag{22}$$

3.4. Extension to Distance-Dependent Propagation Model

In the ANRM model described in previous subsections, it was assumed that the reception of a message that is the only one using a given SC is *always* successful. However, if multiple messages are transmitted in the same SC, reception fails for everyone due to collisions. This is the first assumption listed in Section 3.1. We now relax this model to include a classic propagation model that considers a deterministic gain component based on the distance between the transmitter and receiver, as well as a stochastic component that accounts for fading. This extended model is called DDPM.

Let $G(x)$ be the gain of the used channel when transmitter and receiver are at distance x. We let $G=G_d(x)G_f$, where $G_d(x)=\kappa/x^\alpha$ is the deterministic component of the gain, assumed to follow a power law, and G_f is a random component, accounting for Rayleigh fading. Hence G_f is a negative exponential random variable with mean 1, i.e., $\mathcal{P}(G_f>u)=e^{-u}$ for $u\geq 0$. Let also P_{tx} denote the transmission power level and P_{no} the background noise power level.

The received message is deemed to be decoded correctly if the Signal-to-Noise-plus-Interference Ratio (SNIR) $\Gamma(x)$ exceeds a threshold γ, related to the adopted Modulation and Coding Scheme (MCS), i.e., if

$$\Gamma(x)=\frac{G_fG_d(x)P_{\mathrm{tx}}}{P_{\mathrm{no}}+P_{\mathrm{in}}}\geq\gamma \tag{23}$$

where P_{in} is the interference power level.

Accounting for the Rayleigh fading gain G_f, the probability p_s of the event expressed in Eq. (23) (probability of success, conditional on node transmission) is found to be

$$p_s=\exp\left(-\frac{\gamma}{S(x)}\right)\mathrm{E}\left[\exp\left(-\gamma\frac{P_{\mathrm{in}}}{G_d(x)P_{\mathrm{tx}}}\right)\right] \tag{24}$$

where the expectation is over the interference and

$$S(x)=\frac{G_d(x)P_{\mathrm{tx}}}{P_{\mathrm{no}}}=\frac{\kappa P_{\mathrm{tx}}}{x^\alpha P_{\mathrm{no}}} \tag{25}$$

Interference is modeled using a simple stochastic geometry model, where we consider a receiver located at the origin of a line, a transmitting node, located at distance x of the receiver, and a Poisson field of interfering nodes with mean density λ, measured in nodes per unit length. The geometry considered is on a line, as we refer to a span of road where the length is much greater than the width.

The normalized interference can be expressed as

$$\frac{P_{\mathrm{in}}}{G_d(x)P_{\mathrm{tx}}}=\sum_{y\in\Phi}G_{f,y}\left(\frac{x}{y}\right)^\alpha, \tag{26}$$

where Φ is a Poisson Point Process (PPP) of mean density λ [55]. The expectation appearing in Eq. (26), involving the normalized interference, can be expressed applying Campbell's theorem to the generating function of the PPP of interfering nodes [55]. The result is

$$\mathrm{E}\left[\exp\left(-\gamma\frac{P_{\mathrm{in}}}{G_d(x)P_{\mathrm{tx}}}\right)\right]=\exp\left(-2\lambda x\gamma^{1/\alpha}\frac{\pi/\alpha}{\sin(\pi/\alpha)}\right). \tag{27}$$

If we denote the road length with L, the mean density of interfering nodes is given by $(n-1)/L$ with probability w_n. Here, w_n is the probability that the tagged node is receiving a message transmitted in an SC used by n nodes, one of which is the transmitting node (with distance x from the tagged node) and the other $n-1$ nodes are interfering ones. Out of the N messages transmitted in an RRI, $n\cdot K\tilde{\pi}_n$ are transmitted in an SC that carries n messages, where $\tilde{\pi}_n$, $n=0,1,\ldots,N$, is the steady state probability distribution of the DTMC defined in Section 3.2. Hence, $w_n=(Kn\tilde{\pi}_n)/N$, for $n=1,\ldots,N$. This probability distribution sums to 1 as a consequence of Eq. (12).

Summing up, the interfering node density can be characterized as follows

$$\lambda=\frac{n-1}{L}\quad\text{w.p. } w_n=\frac{Kn\tilde{\pi}_n}{N} \tag{28}$$

Putting together Eqs. (24), (27) and (28), we get the success probability $p_s=p_s(x,P)$:

$$p_s=e^{-\frac{\gamma}{S(x)}}\sum_{n=1}^{N}\frac{Kn\tilde{\pi}_n}{N}\exp\left(-\frac{2(n-1)x\gamma^{1/\alpha}\pi/\alpha}{L\sin(\pi/\alpha)}\right) \tag{29}$$

Note that p_s is a function of the distance x between transmitter and receiver, as well as of the persistence probability P. For nodes randomly scattered along a road of length L, the PDF of the distance between two nodes is $f(x)=\frac{2}{L}\left(1-\frac{x}{L}\right)$, for $0\leq x\leq L$. We can then derive a distance-averaged probability of success as follows:

$$\bar{p}_s(P)=\int_0^L p_s(x,P)f(x)\,dx \tag{30}$$

The failure probability $1-p_s$ can be split according to causes of message reception failure: (i) failure to achieve the required sensitivity level; (ii) failure due to excessive interference. Accordingly, we define the following two conditions:

Failure on sensitivity: $G_fS(x)<\gamma$

Failure on interference: $G_fS(x)\geq\gamma\quad\&\quad\Gamma(x)<\gamma$

Let PLR and CLR denote the probabilities of the two events, respectively. Then, we have

$$\mathrm{PLR}=1-e^{-\frac{\gamma}{S(x)}} \tag{31}$$

$$\mathrm{CLR}=e^{-\frac{\gamma}{S(x)}}-p_s(x,P), \tag{32}$$

where $S(x)$ and $p_s(x,P)$ are given in Eqs. (25) and (29) respectively.

Numerical examples of probability of success as a function of the persistence probability P and of PLR and CLR as function of distance are given in Figs. 2 and 3. Numerical values of the parameters are as follows: $\kappa=6.52\cdot10^{-5}$, $\alpha=2$, $\gamma=20.27\,\mathrm{dB}$, $P_{\mathrm{tx}}=20\,\mathrm{dBm}$,

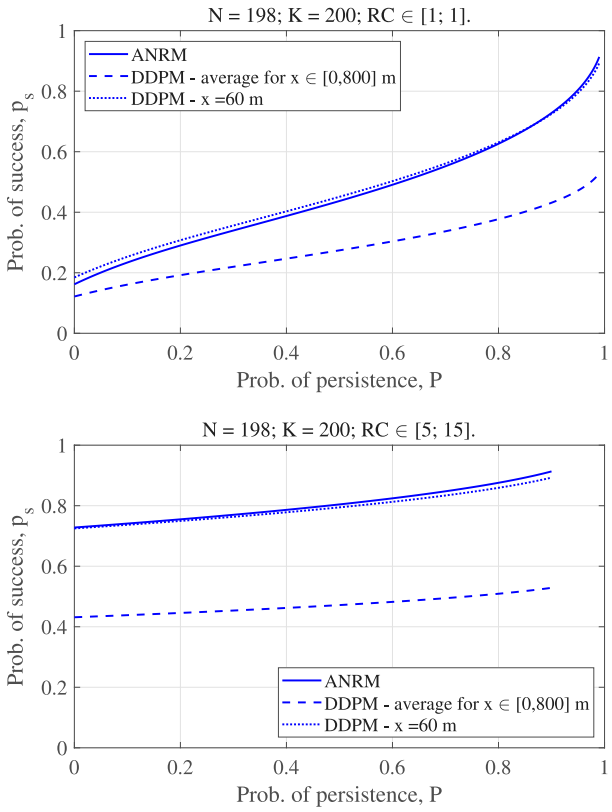

Fig. 2. Probability of success as a function of the probability of persistence P, with ANRM (solid line) and DDPM (dashed and dotted lines) for $N = 198$, $K = 200$. Upper plot: Geometric PDF of the RC. Lower plot: uniform PDF of the RC.

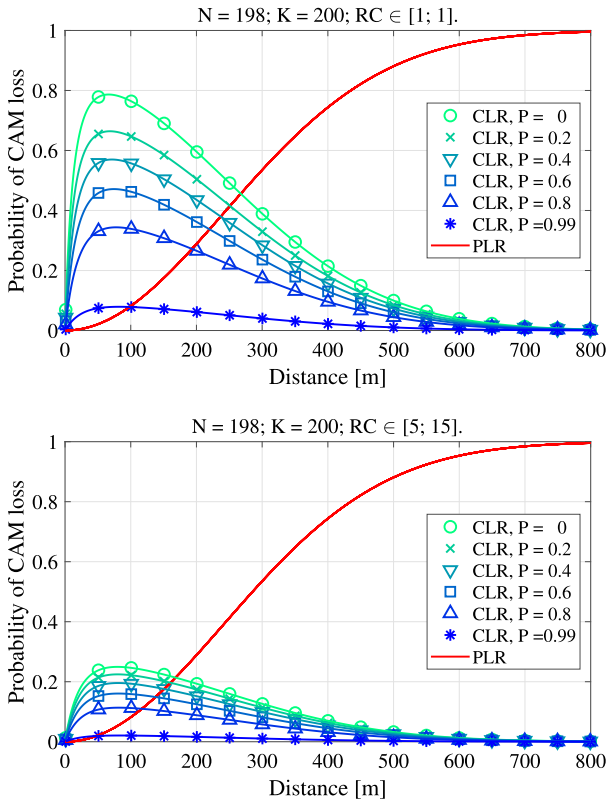

Fig. 3. PLR and CLR as a function of distance x between transmitting and receiving nodes, with DDPM for $N = 198$, $K = 200$. Solid red line: PLR. Solid blue lines with markers: CLR. Upper plot: Geometric PDF of the RC. Lower plot: uniform PDF of the RC. (For interpretation of the references to color in this figure legend, the reader is referred to the web version of this article.)

$P_{\text{no}} = -98.83\,\text{dBm}$, $L = 800\,\text{m}$, RRI of 100 ms. These values correspond to using 2 TBs per time slot, TB made up of 23 RBs, with an overall bandwidth equal to 4.14 MHz, assuming a noise figure of 9 dB, thermal noise power spectral density of $-174\,\text{dBm}\,\text{Hz}^{-1}$, and carrier frequency at 5.9 GHz.

Fig. 2 show p_s as a function of P for the ANRM and DDPM models, for $K = 200$ SCs and $N = 198$ nodes. The success probability for ANRM (solid line) is computed according to Eq. (13). The average success probability for DDPM (dashed line) is computed according to Eq. (30). The success probability for a fixed distance of 60 m is shown as well (dotted line), computed according to Eq. (29) with $x = 60\,\text{m}$. Fig. 2(a) is obtained using the Geometric PDF for the RC, while the uniform PDF is used for the RC in Fig. 2(b).

A significant discrepancy of quantitative values (not of qualitative behavior however) is noticed comparing ANRM and DDPM results, when averaged over the distance between transmitter and receiver. However, DDPM yields results close to ANRM if we set a distance of 60 m, with is 1/10 of the considered road length. The result confirms that ANRM is reliable when considering relatively close nodes. From the point of view of vehicular communications, this is actually the most critical part of a vehicle neighborhood.

Fig. 3 plots $p_s(s, P)$ decomposition into PLR and CLR as a function of x, for several values of the persistence probability P, for $K = 200$ SCs and $N = 198$ nodes. Fig. 3(a) is obtained using the Geometric PDF for the RC, while the uniform PDF is used for the RC in Fig. 3(b).

A first important aspect is that message successful reception is no more a black-or-white outcome, according to whether a collision does or does not occur. There is instead a soft increase of the probability of message loss, exhibiting a phase-transition behavior (at least for PLR), when the distance between transmitter and receiver grows. With DDPM collisions turn into interference, that can impair successful reception, in case it is large enough.

Moreover, these results allow an interesting insight into the causes that lead to message losses. For small values of distance x, the PLR is essentially zero, meaning that the sensitivity requirement is always met. Interference has a marginal effect, but it rapidly increases for small to medium distances, becoming the dominant reason for message loss. However, as the distance grows further (beyond a few hundred meters in our case), loss is definitely dominated by attenuation, hence PLR is overwhelming with respect to CLR.

To complete the discussion of the extension of the analytical model introduced in this section, we must address one final point. The derivation of p_s in Eq. (29) uses the probability distribution $\bar{\pi}_n$, $n = 0, 1, \ldots, N$, which is the steady state probability distribution of the mean-field approximation DTMC defined in Section 3.2. Can we apply this DTMC to describe the occupancy level of SCs in the current modeling framework, where we replace the ANRM model with a DDPM model? The question is not trivial, since the (re-)selection of the SC for transmission is done based on sensing, i.e., the amount of power received in that SC by the node that is making its (re-)selection. In fact, the DTMC defined in Section 3.2 can be considered a reasonably accurate approximation even with DDPM, provided that the sensing threshold is set to the noise power level only. More specifically, for a road span of length L, the maximum distance between two nodes is L. Taking into account fading, the probability that a tagged node could hear a node transmitting in an SC at the farthest distance is given by $\exp\left(-\frac{P_{\text{no}}}{\kappa P_{\text{tx}}/L^{\alpha}}\right)$. For example, using the numerical parameters of this section, the probability that a node can detect a busy SC, even if it is being used by a single, most distant other node, is ≈0.95. This high level of detection probability justifies the use of the DTMC defined in Section 3.2. This conclusion holds for a road span length on the order of the channel reuse distance.

Table 3
Main simulation parameters and settings.

Parameter	Value
Number of nodes	195
Number of SCs per allocation period	200
RRI	100 ms
RC	[5;15]

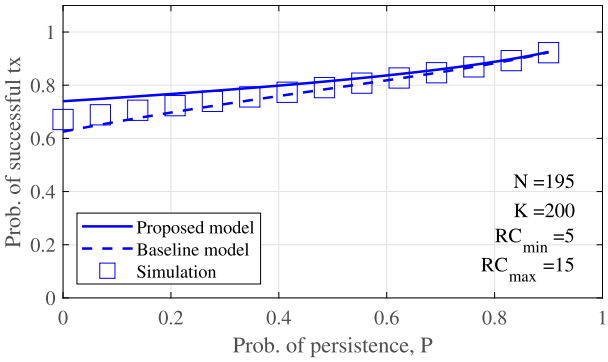

Fig. 4. Probability of a successful transmission as a function of persistence probability. Analytical models versus simulation (square markers).

4. Analytical model: validation and evaluation

In this section, we evaluate the performance of the SPS using our analytical model and MATLAB simulations. The evaluation helps to determine the conditions under which the best system performance is achieved on key performance metrics, and evaluates the accuracy and reliability of the proposed analytical model. Specifically, we describe the simulation settings (shown in Table 3) and metrics and compare the performance of the SPS algorithm for a set of N nodes sharing K SCs for three different approaches: *Proposed model* (described in Section 3), MATLAB-based *Simulation model*, and *Baseline model* (inspired by the modeling approach proposed in [53]). In terms of performance metrics, we consider the transmission success probability, the PAoI, and the average AoI metrics.

4.1. Simulation model

The simulation implements the model described in Section 3. It generates the RC with its standard probability distribution (uniform between $RC_{\min}$ and $RC_{\max}$). All time quantities are normalized with respect to the duration of one RRI and are therefore expressed as multiples of the RRI.

As long as a node is the only one using an SC and messages are regularly delivered without error, its AoI will grow from zero to one RRI every RRI. If multiple nodes simultaneously decide to select an SC for subsequent use, there is a possibility that they will select the same SC, resulting in interference and failed messages. In these cases, the AoI of such nodes increases dramatically and depends on the value of the RC selected by each node. The level of AoI is critical to the safe operation of real-time safety applications and services, since nodes may not be able to receive messages from their neighbors for a critically long period of time.

The WBS issue [31] is accounted for by Matlab simulations, to verify its impact on the analytical model accuracy.

4.2. Result analysis

Fig. 4 shows the probability of successful transmissions as a function of the persistence probability P for the three considered approaches. Parameters values are $N = 195$, $K = 200$, the RC is uniformly distributed between 5 and 15, hence with an average value of 10.

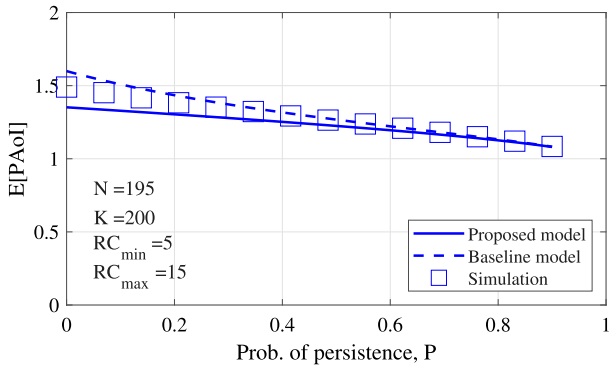

Fig. 5. Average PAoI as a function of persistence probability. Analytical models versus simulation (square markers).

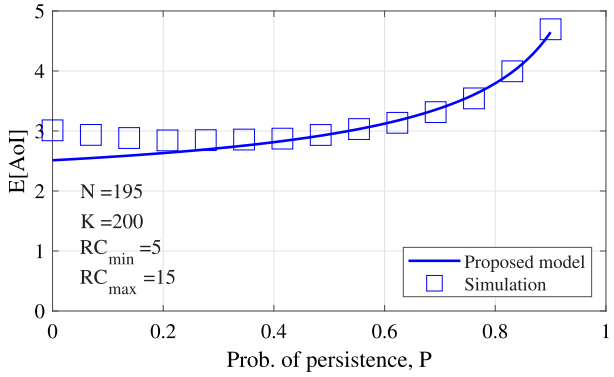

Fig. 6. Average AoI as a function of persistence probability. Analytical models versus simulation (square markers).

It can be seen that both the Proposed and Baseline models are very accurate, i.e., they agree very well with the simulation results. The Proposed model is only slightly less accurate for low persistence probability values. This is due to the Geometric approximation retained in the model to draw the RC value, as opposed to the Uniform probability distribution proposed in the ETSI standard. It should be noted, however, that using the Geometric probability distribution actually *improves* performance, i.e., we can observe a higher probability of successful transmissions.

These observations are also confirmed by the performance of PAoI and AoI in the following figures. In particular, Fig. 5 shows the PAoI as a function of the persistence probability P. The mean PAoI is measured in units of RRI. Again, the selection of the RC value using a Geometric distribution not only leads to an accurate estimation of the PAoI compared to simulations, but it actually decreases the obtained PAoI.

The average AoI versus P is shown in Fig. 6. Similar to the previous results, replacing the RC probability distribution (Uniform, according to the standard) with a Geometric probability distribution, as done in our Proposed model, improves the AoI performance. Our model turns out to provide quite good accuracy, at least for medium to high persistence probability values.

In the following, still assuming a Geometric probability distribution for the RC, we can equivalently redefine the persistence algorithm by replacing RC and the persistence probability P by a unique parameter $q = (1-P)/\overline{RC}$ and say that the same SC is maintained with probability $1-q$ at the end of each RRI. With probability q, a new SC is selected. In other words, the persistence interval is a Geometrically distributed multiple of the RRI. As for the simulations, we set the minimum and maximum values of RC to 1, so that $\overline{RC} = 1$.

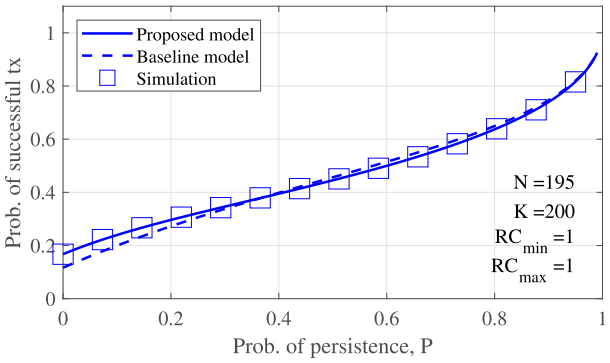

Fig. 7. Probability of a successful transmission as a function of persistence probability. Analytical models versus simulation (square markers).

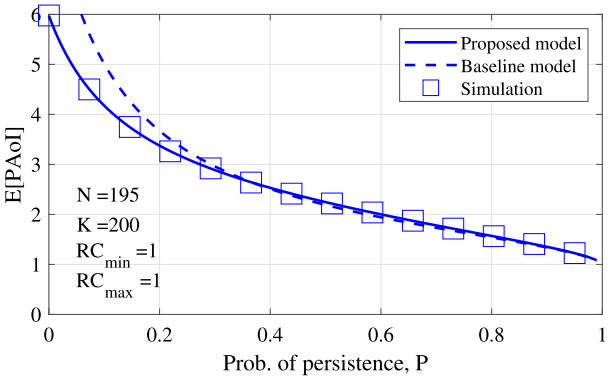

Fig. 8. Average Peak AoI as a function of persistence probability. Analytical models versus simulation (square markers).

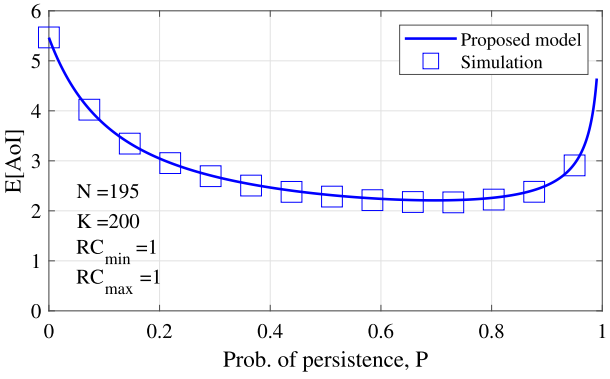

Fig. 9. Average AoI as a function of persistence probability. Analytical models versus simulation (square markers).

The probability of successful transmission, average PAoI and average AoI are plotted as a function of the persistence probability $P = 1-q$ in Figs. 7 to 9, respectively.

Two main remarks are in order. First, the Proposed model is very accurate for all metrics considered. Second, a new qualitative behavior emerges from the analysis of AoI that has not been noticed in previous works: AoI performance is not monotonic with the persistence probability. On the contrary, an optimal value appears that corresponds to about 0.7. The intuition that explains this result is as follows. For low values of the persistence probability, nodes change their selected SC hectically, causing multiple collisions. As a result, the inter-message delivery time has a large variance, which results in a large AoI. For very high values of the persistence probability, most of the time a node is successful and delivery of update messages occurs regularly at the rate of one new message per RRI. However, once the node enters a collision state, it maintains it for a long time (high persistence). The resulting delivery process is a kind of ON–OFF communication channel, where long OFF times occur from time to time. While this does not affect the mean inter-message delivery time too much (hence the PAoI decreases monotonically with P), it does affect the variance of the inter-message delivery time significantly (hence the AoI increases steeply for large P).

5. Analysis in a highway environment

In this section, we delve into the realistic simulation parameters used in the ns-3 simulator [56], including simulation calibration, metrics, and a comprehensive comparison of SPS performance under different system settings.

In particular, to validate the accuracy of our proposed analytical model, we conducted simulations of the SPS mechanism in more authentic scenarios using the ns-3 network simulator and the MoReV2X module [57,58]. MoReV2X serves as a dedicated simulator for sub-6 GHz NR-V2X communications within the ns-3 framework. Its focus is on the implementation of NR-V2X Mode 2, which uses a distributed access strategy to allow direct data exchange between vehicles.

5.1. Key performance metrics

In conjunction with the definition of traffic and channel models, 3GPP introduced performance metrics for the analysis of NR-V2X communications [59]. In our analysis, we focus on the metrics described below.

5.1.1. Packet delivery ratio

For broadcast communications, the initial metric is PRR type 1. In this paper, we will refer to this metric as PDR. Within the region where the vehicle distances from the transmitting UE are in the range $[a, b]$, the PDR for each transmitted packet is evaluated as $\frac{Y}{Z}$, where Y is the number of UEs in the region that successfully receive the packet, and Z is the total number of receiving UEs in the same region. Assuming that M packets are generated during the simulation, the average PDR is computed as:

$$PDR = \frac{\sum_{j=1}^{M} Y_i}{\sum_{j=1}^{M} Z_i},$$

with $a = i \cdot 50\,\text{m}$, $b = (i+1) \cdot 50\,\text{m}$, and $i = 0, 1, \ldots, 18$.

Note that the size of the region has been increased compared to the standard in order to obtain more relevant statistics based on the results of the simulations.

5.1.2. Collision Loss Ratio and Propagation Loss Ratio

CLR and PLR are metrics used to assess the impact of collisions and propagation losses on the reliability of communications over a given distance range $[a, b]$. These metrics provide insight into the specific challenges that affect communication within the specified distance range. CLR reflects the impact of collisions, while PLR reflects the impact of poor propagation conditions on the reliability of the communication system.

CLR is a metric that quantifies the ratio of packets lost due to collisions within the distance range $[a, b]$ to the total number of packets transmitted within that range. Mathematically, CLR is expressed as:

$$CLR = \frac{N_{\text{CL}}}{N_{\text{PL}} + N_{\text{CL}} + N_{\text{SR}}}. \tag{33}$$

PLR is a metric that quantifies the ratio of packets lost due to poor propagation conditions (insufficient Signal-to-Noise Ratio (SNR)) within the distance range $[a, b]$ to the total number of packets transmitted within that range. Mathematically, PLR is expressed as:

$$PLR = \frac{N_{\text{PL}}}{N_{\text{PL}} + N_{\text{CL}} + N_{\text{SR}}}, \tag{34}$$

where N_{PL} is the number of packets received incorrectly within the same range because of poor propagation conditions (i.e., the number of packets that did not collide but experienced an insufficient received SNR), N_{CL} is the number of packets in the $[a, b]$ distance range that were lost in a collision and could not be successfully retrieved because of an insufficient SNIR, and N_{SR} is the number of correctly received packets within the same range.

5.1.3. Peak age of information

For a given transmitter–receiver pair, the PAoI is defined as the time between two consecutive successful receptions of packets belonging to the same application flow when the transmitter–receiver distance falls within the $(0, D_{max}]$ range, where D_{max} is a fixed manageable value, at the time of reception.

5.1.4. Age of information

AoI is the age of the most recent piece of information received from a remote source that sends updates.

$$\mathrm{E}[AoI] = \lim_{T\to\infty} \frac{1}{T} \int_0^T AoI(t)\, dt = \lim_{N\to\infty} \frac{\sum_{k=1}^{N} \frac{1}{2} Y_k^2}{\sum_{k=1}^{N} Y_k} \tag{35}$$

where Y equal to PAoI.

$$\mathrm{E}[AoI] = \frac{\mathrm{E}[PAoI^2]}{2 \cdot \mathrm{E}[PAoI]} \tag{36}$$

5.2. Calibration of simulations

To obtain relevant simulation results in more realistic scenarios, it is necessary to define some simulation parameters depending on the MCS used and the channel configuration. In this case, we configure the channel so that the number of resources K available for reservation and transmission within an RRI is equal to 200 (as in Section 4.2). To obtain the relevant values of the thresholds of the rxSensitivity, RSSI, RSRP and awareness range R_{aw}, we use MCS with index 13 (16QAM-0.5). These values have a significant impact on key performance metrics and the evaluation of simulation results, so we detail the process of obtaining these thresholds in this section.

5.2.1. rxSensitivity threshold

A new generic term, $\overline{R}_{\text{eff Tx}}$ (effective data rate), is proposed in [60], which can be applied to any wireless protocol, assuming a constant Packet Error Rate (PER). Physical meaning of $\overline{R}_{\text{eff Tx}}$ is obtained from TB size in bits (TBS_{MCS}), which is defined depending on the MCS and the packet error rate limit PER set to 10% according to Eq. (37):

$$\overline{R}_{\text{eff Tx}} = \frac{TBS_{MCS}}{1000} \cdot (1 - PER) \tag{37}$$

where TBS_{MCS} is calculated using the formulas for MCS index equals to 13 presented in [61] and $\frac{TBS_{MCS}}{1000}$ is the maximum throughput in Mb/s.

Receiver sensitivity values can be compared to a generic receiver sensitivity limit. The equation for the generic receiver sensitivity limit is:

$$rxSensitivity = 10 \cdot \log_{10} \cdot (2^{\frac{\overline{R}_{\text{eff Tx}}}{4}} - 1) - 81.3\,\text{dB}. \tag{38}$$

We assume a channel bandwidth equal to 10 MHz, an MCS index equal to 13, and a numerology number $\mu = 0$. For the given bandwidth structure of the channel we have the following: the number of available RBs is 52, the size of each SC (SC_{size}) can be configured with {10,12,15,20,25,50} RBs, which leads to the total number of SCs available for resource allocation (N_{SC}) to {5,4,3,2,2,1} respectively. According to [61], the total number of RBs formed SC ($N_{\text{SC}} \cdot SC_{\text{size}}$) affects the TBS_{MCS}, which leads to different values of rxSensitivity for different configurations of the communication channel. rxSensitivity calculation results are presented in Table 4.

Table 4
RSSI, RSRP, and rxSensitivity thresholds for different configurations of the channel (10 MHz bandwidth and $\mu = 0$).

N_{RB}	SC_{size}	N_{SC}	$RSSI_{\text{th, dBm}}$	$RSRP_{\text{th, dBm}}$	$rxSensitivity$, dBm
52	10	5	−100.42	−121.21	−84.71
52	12	4	−99.45	−121.03	−83.59
52	15	3	−98.31	−120.86	−82.16
52	20	2	−96.89	−120.70	−80.12
52	25	2	−95.83	−120.24	−78.56
52	50	1	−92.63	−120.42	−72.07

5.2.2. RSSI and RSRP thresholds

Sidelink (SL) RSSI is a measure of the average power received in a specific SC during certain time slots. It helps in determining the SL Channel Busy Ratio (CBR). SL CBR for a slot is the proportion of SCs in the resource pool where the received signal strength measured by the device is above a set threshold during a specific measurement window. This window is determined by the parameter timeWindowSize-CBR and is represented as $[n - a, n - 1]$, where a is either 100 slots or $100 \cdot 2\mu$ slots.

RSRP is the average power of the resource elements carrying demodulation reference signals for the physical sidelink shared channel. These signals are organized in TBs transmitted on the Physical Sidelink Shared Channel (PSSCH). The RSRP value, specified in the technical standard [62], is used at the MAC layer for sensing procedures.

The relationship between RSRP and RSSI is given by Eq. (39):

$$\text{RSRP} = \text{RSSI} - 10 \cdot \log_{10}(12 \cdot SC_{\text{size}}) \tag{39}$$

In the SPS mechanism, a UE assesses RSRP from other UEs based on the SCI. The UE saves this information and utilizes it to decide which candidate resources to exclude when triggered for a new selection. Exclusions are determined by both the UE's own RSRP measurements and reservations received from other UEs. Candidate resources are excluded only if the measured RSRP associated with the reservation is higher than a configured threshold, with thresholds set in the resource pool.

After excluding resources in step 1, the UE (using DS or SPS) checks if the remaining available candidate resources in the selection window are equal to or higher than a specified percentage (X%). Otherwise, the RSRP thresholds are increased by 3 dB, and the process is repeated iteratively until the percentage of available candidate resources in the selection window reaches at least X%. Possible values for X include 20, 35, or 50, determined by the priority of the TB for which the UE is selecting new SL resources.

To calculate RSSI and RSRP thresholds we are using Eqs. (39) and (40).

$$\begin{aligned}\text{RSSI}_{\text{threshold}} = {} & N_{\text{thermal}} + N_{\text{f}} + N_{\text{m}} \\ & + 10 \cdot \log_{10}(RB_{\text{f}} \cdot RB_{\text{data}}),\end{aligned} \tag{40}$$

where N_{thermal} is the thermal noise equal to −174 dBm, N_{f} is noise figure equal to 9 dBm, N_{m} is the noise margin that equals to 3 dBm, RB_{f} is the bandwidth of a RB equal to 180 kHz, and RB_{data} is the number of RBs that carry data in the configured channel, which is equal to $SC_{\text{size}} - 2$. RSSI and RSRP calculation results are presented in Table 4.

5.2.3. Awareness range

To emulate the constraint of the analytical model (where all nodes can hear each other), it is essential to determine the parameter R_{aw}, which represents the distance within which nodes can reuse SCs if they are located at a distance greater than R_{aw}. To achieve this, a series of simulations were conducted with a single pair of nodes, with the distance between them gradually increasing throughout the simulation. The parameters for this particular simulation are outlined in Table 5.

Fig. 10 illustrates the total received power versus distance in two formats for comparison with rxSensitivity, RSSI thresholds, and RSRP

Table 5
Simulation parameters for one pair of nodes.

Parameter	Values
Number of nodes, N	2
Highway length	5 km
Number of lanes	2
Vehicles' speed	70 km h^{-1}
OFDM numerology μ	0
SCS	15 kHz
Time slot duration t_s	1 ms
RRI	100 ms
T_{gen}	100 ms
Channel bandwidth, BW	10 MHz
Subchannel size, SC_{size}	25 RBs
Available subchannels, N_{SC}	2
Available resources per RRI, K	200
MCS	16QAM-0.5 (MCS13)
Transmission power	20 dBm and 23 dBm
rxSensitivity	−78.56 dBm
RSSI threshold	−95.83 dBm
RSRP threshold	−120.24 dBm
RC range	[5;15]
Probability of persistence, P	0.8

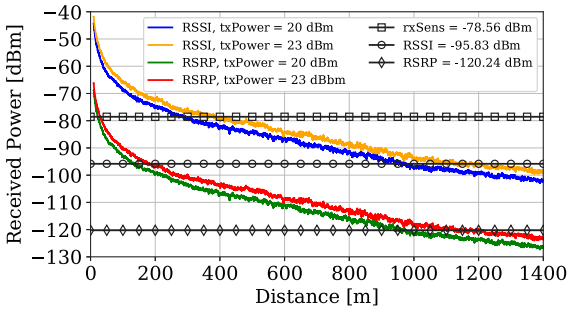

Fig. 10. Total received power as a function of distance for one pair of nodes. (For interpretation of the references to color in this figure legend, the reader is referred to the web version of this article.)

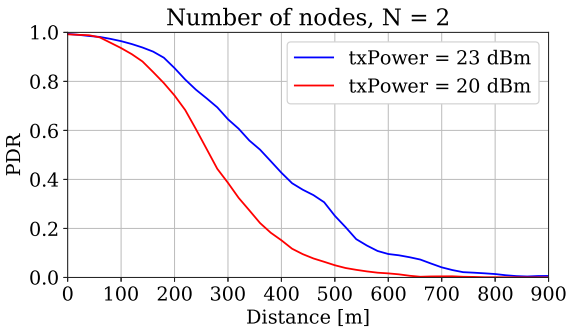

Fig. 11. PDR as a function of distance for one pair of nodes.

Table 6
Parameters for simulation.

Parameter	Values
Number of nodes, N	200
Highway length	920 m
Number of lanes	4
Vehicles' speed	70 km h^{-1}
OFDM numerology, μ	0
SCS	15 kHz
Time slot duration, t_s	1 ms
RRI	100 ms
T_{gen}	100 ms
Channel bandwidth, BW	10 MHz
Subchannel size, SC_{size}	25 RBs
Available subchannels, N_{SC}	2
Available resources per RRI, K	200
MCS	16QAM-0.5 (MCS13)
Transmission power	20 dBm
rxSensitivity	−78.56 dBm
RSSI threshold	−95.83 dBm
RSRP threshold	−120.24 dBm
RC	1
Probability of persistence, P	[0; 0.99]

threshold. The orange and red curves represent the received signal power when the transmitted signal power is set to 20 dBm, while the blue and green curves correspond to a transmitted power of 23 dBm. Distinctively marked black lines represent the thresholds for RSSI (∘ marker), RSRP (⋄ marker), and receiver sensitivity (□ marker).

The points of intersection between the received signal curves and the boundary lines determine the distances R_{aw} at which a signal of a specified level becomes detectable during the sensing procedure and measurement of the CBR. In addition, these intersections determine the maximum distance R_{dec} between nodes that ensures successful packet transmission and decoding. For a transmitter signal power of 23 dBm, the awareness range R_{aw} is 1150 m, while the maximum decoding distance R_{dec} for probable successful packet transmission and decoding is 400 m. For a transmitter with a power of 20 dBm, these values become 920 m and 300 m, respectively. Note that successful reception and decoding can occur beyond R_{dec}, but the probability of such events is less satisfactory.

The impact of distance on the PDR is depicted in Fig. 11. Given the participation of only two nodes in this scenario, collisions do not influence the PDR. Instead, losses primarily arise due to signal attenuation over varying distances. To streamline subsequent simulations involving a larger number of vehicles and mitigate complexity, we opt for a transmitter signal strength of 20 dBm.

5.3. Simulation setup

The scenario analyzed consists of a 920 m section of highway with two lanes in each driving direction. The vehicles maintain a speed of 70 km h^{-1}, for a total of 200 veh, corresponding to the available SCs per RRI.

Throughout the simulations, the Orthogonal Frequency-Division Multiple Access (OFDM) numerology is set to 0, resulting in a Sub-Carrier Spacing (SCS) of 15 kHz and a slot duration of $t_s = 1$ ms. NR-V2X radios are configured to operate on a 10 MHz channel within the 5.9 GHz Intelligent Transportation Systems (ITS) band, using SCs of 25 RBs. As a result, there are two SCs available in each time slot, which allows us to say that the number of K resources available for allocation (in the form of SCs) in the time period equal to RRI is 200. Transmission occurs with 16QAM-0.5 MCS. After calibrating the simulation parameters (see Section 5.2), the transmit power is set to 20 dBm, the receiver sensitivity is set to −78.56 dBm, and the RSSI threshold is set to −95.83 dBm. Pathloss and shadowing follow the models described in [59]. To consider fast-fading impairments affecting the TB and SCI Physical Layer performance, MoReV2X incorporates Block-Error Rate (BLER) curves from [63,64], respectively.

At the MAC sublayer, T_0 is set to a number of slots equivalent to 1100 ms, the initial RSRP threshold is set to −120.24 dBm, and β is set to 20%. In SPS, the persistence probability value varies within the range $P \in [0; 0.99]$ in increments of 0.1. For optimal SPS performance, periodic traffic is employed with a message generation interval of $T_{\text{gen}} = 100$ ms. The periodic traffic model employs 190 Byte packets, guaranteeing the reservation of only one SC for transmission (same as in the analytical model). The WBS [31] effect is taken into account in the ns-3 MoReV2X simulator.

To understand the impact of persistence on key performance metrics in this simulation, we use a constant value for RC, set to 1. This choice is made because setting $RC = 1$ allows us to observe the

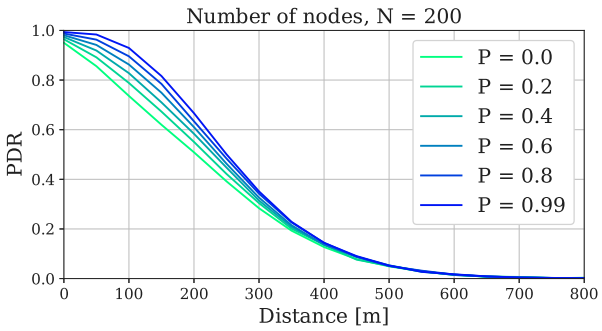

Fig. 12. PDR as a function of distance. (For interpretation of the references to color in this figure legend, the reader is referred to the web version of this article.)

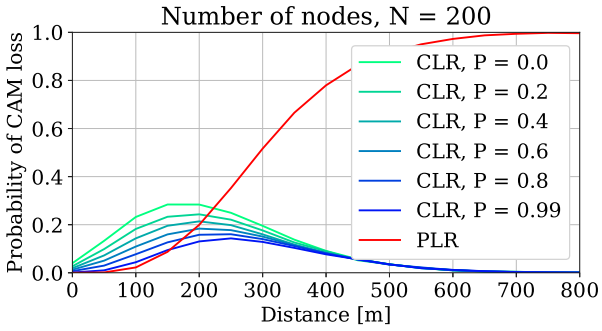

Fig. 13. Probability of CAM loss as a function of distance. (For interpretation of the references to color in this figure legend, the reader is referred to the web version of this article.)

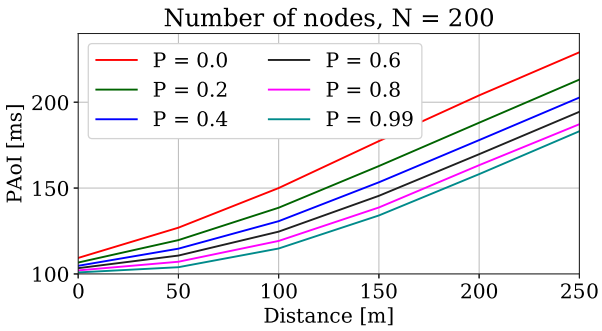

Fig. 14. PAoI as a function of distance.

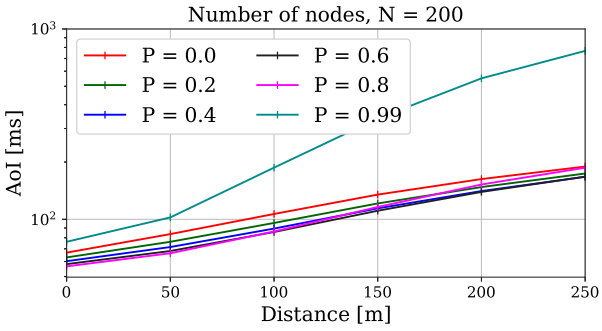

Fig. 15. AoI as a function of distance (log-scale).

performance of *pure* persistence. With $P = 0$, we examine the operation of DS, and with $P > 0$, we assess the functionality of SPS with *pure* persistence. Using a uniform PDF of RC values in the range [5;15], we observe an *enhanced* persistence. Even when $P = 0$, the average number of time slots reserved for transmission is $\overline{RC} = 10$ (representing SPS with built-in persistence). For values of $P > 0$, we introduce additional persistence, where the average number of time slots reserved for transmission becomes $(1 - P)\overline{RC}$. Key simulation parameters are summarized in Table 6.

5.4. Distance-dependent performance evaluation

In this section, we look at the correlation between key performance metrics and the distance between nodes over different persistence probability values. The results stem from simulations, the details of which are described in Section 5.3. It is important to emphasize that these results were obtained for a fixed RC value of 1. This fixed RC value allows for a deeper and more detailed understanding of the impact of persistence on key performance metrics in the context of 5G NR-V2X.

Fig. 12 illustrates the PDR versus distance, with different colors representing different persistence probability settings. Notably, a higher persistence probability correlates with an improved PDR, and a persistence probability of 0 yields the worst results. It is worth noting that this graph helps determine the distance at which the average probability of successful message delivery is satisfactory. For this simulation scenario, a distance value of $D_{\max} = 200\,\text{m}$ is highlighted, which achieves an average success rate of 60%. This value serves as the basis for analysis of PAoI and AoI, as statistics beyond $D_{\max}$ become less relevant for safety considerations. The focus is on the freshness of information from nearby nodes, ignoring potentially high losses for sufficiently distant nodes.

Fig. 13 presents the probability of message loss due to collisions (CLR) and propagation (PLR) as a function of distance. The PLR (solid red line) is independent of the persistence probability because persistence cannot affect the physical nature of signal propagation. Different shades of blue to cyan lines represent the CLR at different persistence probability values, revealing local maxima in each case. Peaks in the CLR curves occur at distances between nodes where propagation losses are rare, but reception fails when excessive interference is present. In this range of transmitter-to-receiver distances, the dominant cause of packet loss is due to simultaneous transmissions using the same SC, namely collisions. Beyond the CLR peak, attenuation definitely becomes the dominant source of failed reception, and collisions are less important. In other words, beyond about 400 m, any provision we could define for the multiple access (e.g., a smarter variant of SPS) would have a limited impact, since successful packet delivery is mainly affected by the physical layer attenuation. We will see that increasing the transmit power level has controversial effects. On the one hand, it improves the range over which a strong enough signal can be received. On the other hand, it increases the effects of interference.

Comparing Fig. 13 with Fig. 3(b), which shows the results from the analytical model in Section 3.4, it is possible to see that the qualitative behavior matches. However, the quantitative agreement is not as good. There are two main reasons why the extended analytical model does not fully agree with the simulations. First, the propagation model in ns-3 assumes log-normal shadowing, while the stochastic geometry model considered in Section 3.4 requires Rayleigh fading to maintain analytical tractability. Second, the analytical model in Section 3.4 assumes that the RSSI level used for sensing is equal to the noise floor level. This allows the DTMC model defined in Section 3 to be used. However, the RSSI level in ns-3 includes a margin above the noise floor. More importantly, since the propagation model includes a randomized component (log-normal shadowing), there is a nonzero probability of exceeding or not exceeding this threshold, which cannot be accounted for in the DTMC model.

Figs. 14 and 15 show PAoI and AoI as a function of distance. The distance analysis is capped at $D_{\max}$, which ensures minimally satisfactory probabilities of successful message transmission over various persistence probabilities. PAoI exhibits a monotonic increase with

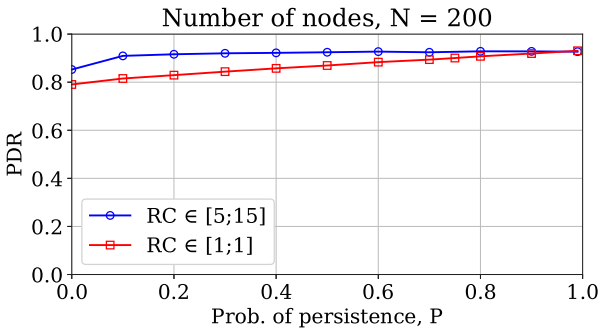

Fig. 16. Mean PDR as a function of probability of persistence for distances less than 200 m. (For interpretation of the references to color in this figure legend, the reader is referred to the web version of this article.)

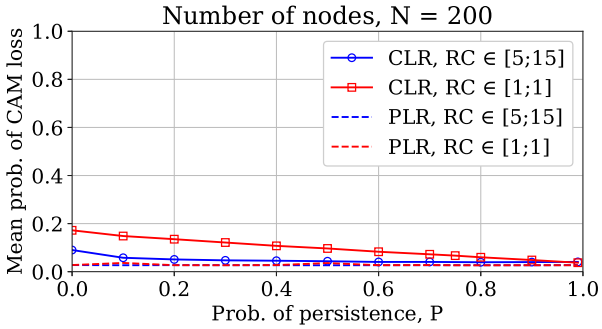

Fig. 17. Mean probability of message loss as a function of probability of persistence for distances less than 200 m.

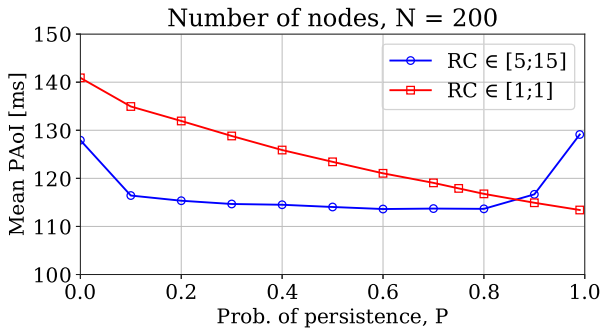

Fig. 18. Mean PAoI as a function of probability of persistence for distances less than 200 m.

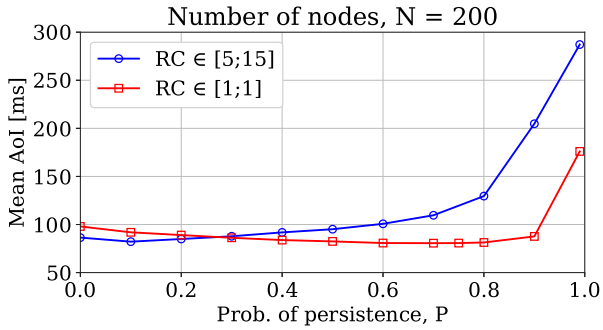

Fig. 19. Mean AoI as a function of probability of persistence for distances less than 200 m.

the distance between nodes, illustrating the increasing values of CLR and PLR from 0 m to 200 m. Once again, the maximum persistence probability proves to be the most effective, manifesting fewer collisions and a higher probability of successful packet transmission.

The AoI in Fig. 15 is plotted on a logarithmic scale for better visualization. Unlike the PAoI, the AoI demonstrates a different behavior. A persistence probability of 0.99 shows the worst AoI value, which increases sharply with distance. Persistence probability values from 0 to 0.8 show overlap at different distances. The minimum AoI value at 50 m is achieved with a persistence probability of 0.8, and it drops to 0.6 at distances greater than 100 m. This behavior prompts a detailed investigation of dynamic persistence probability management algorithms based on the distance between nodes to minimize the average AoI.

5.5. Persistence-dependent performance evaluation

In this section, we examine key performance metrics as a function of persistence probability. For each persistence probability value, the key performance metric values are averaged relative to the distance between nodes. This involves considering the weight coefficients of each distance region to derive pertinent values, building on the statistical analysis from the modeling results in Section 5.4. Similar to the analytical model (see Section 3), we use the same simulation setup (see Table 6). Two approaches to determining RC values are explored: a fixed RC set to 1 (shown by the red line) and an RC in the range [5;15] (shown by the blue line) using a uniform PDF, following standard practices. All values are computed for nodes positioned at a distance equal to or less than D_{max}.

Fig. 16 illustrates the mean probability of successful packet transmission, while Fig. 17 shows the mean probability of losses due to collision or propagation. PDR exhibits monotonic behavior, with the uniform PDF of RC showing optimal efficiency for all persistence probability values. Notable, for a uniformly distributed RC, PDR remains nearly unchanged for persistence probability values from 0.1 to 0.99. A persistence probability value of zero demonstrates the poorest PDR performance. PLR, as expected, remains constant relative to the persistence probability, with a value close to zero due to the negligible influence of propagation at small distances between nodes. Consequently, CLR mirrors PDR in Fig. 16 and shows monotonic behavior. The approach with a uniform PDF of RC reduces collisions by distributing cases of resource changes over time, thus avoiding simultaneous resource changes as observed with RC set to 1. Once again, a persistence probability of zero shows the worst performance among of all values examined.

Fig. 18 shows PAoI, where the behavior for the case with a uniform PDF of RC is non-monotonic, contrary to the analytical model, with a minimum at a persistence probability of 0.6 (for the obtained accuracy of the persistence probability). The absolute difference between the maximum and minimum values of PAoI is 15 ms. As the scale increases, this non-monotonic behavior converges to a linear trend, as observed in the developed analytical model. On the other hand, the fixed RC approach exhibits monotonic PAoI behavior and lags behind the uniform PDF of RC for persistence probability values below 0.87.

Fig. 19 shows the AoI as a function of persistence probability for different approaches to RC formation. Notably, both approaches display non-monotonic AoI behavior with the presence of minima: for $RC \in [1;1]$, between 0.6 and 0.7, and for $RC \in [5;15]$, with a value of 0.1. This is consistent with the behavior of AoI in our analytical model.

Fig. 20 depicts a comparative analysis between the performance of the extended analytical model and corresponding simulations in ns-3 with a uniform probability distribution of RC, as prescribed in the SPS standard. The focus is on the probability of successful message delivery and the mean PAoI, since these metrics can be computed by using the extended analytical model. It is evident that the extended model is able to capture the complexity of the realistic propagation environment, giving quite accurate performance predictions as compared to ns-3 simulations. On the contrary, the evaluation of the mean AoI requires further model development, which is beyond the scope of this paper and will be addressed in future work.

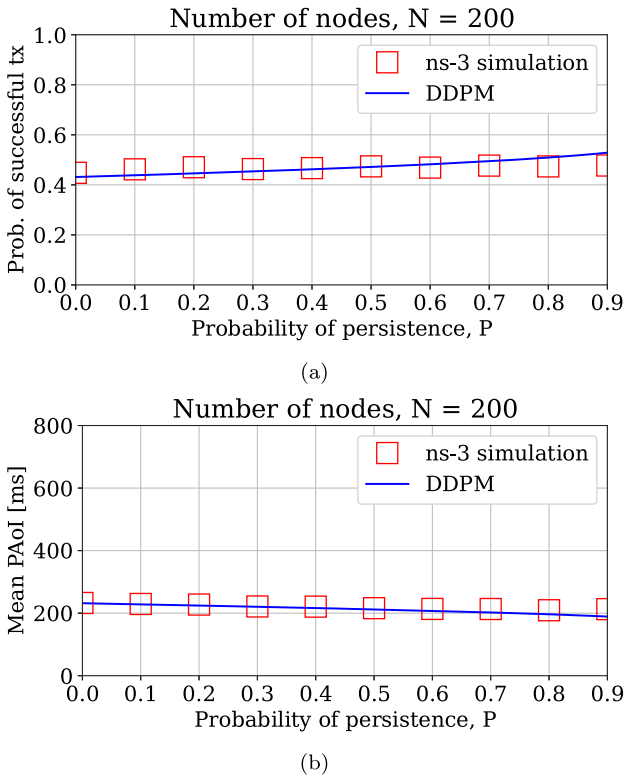

Fig. 20. Comparative analysis of (a) transmission success probability, and (b) mean PAoI between analytical model and ns-3 simulations with $RC \in [5; 15]$ and for distances less than 800 m.

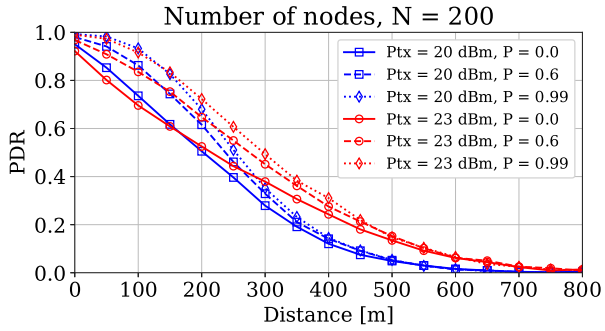

Fig. 21. PDR as a function of distance. (For interpretation of the references to color in this figure legend, the reader is referred to the web version of this article.)

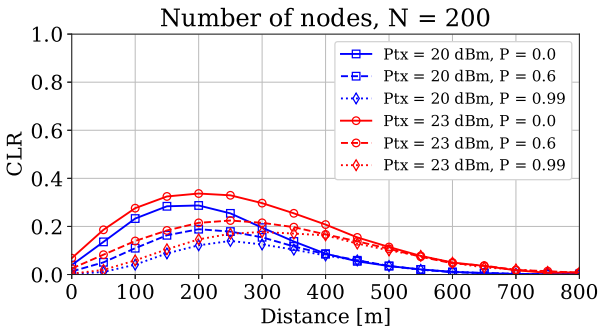

Fig. 22. CLR as a function of distance. (For interpretation of the references to color in this figure legend, the reader is referred to the web version of this article.)

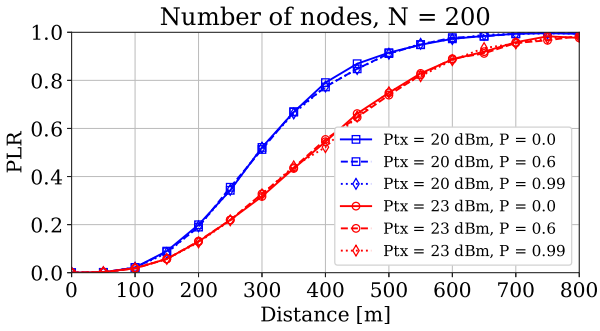

Fig. 23. PLR as a function of distance. (For interpretation of the references to color in this figure legend, the reader is referred to the web version of this article.)

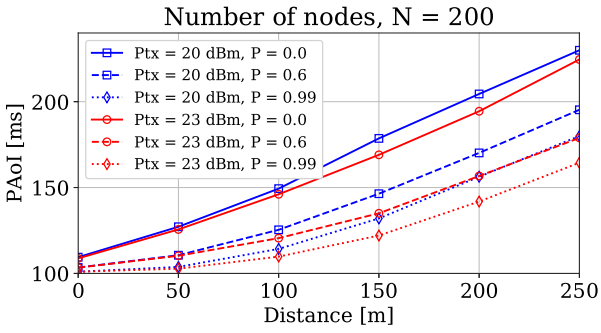

Fig. 24. PAoI as a function of distance. (For interpretation of the references to color in this figure legend, the reader is referred to the web version of this article.)

5.6. Evaluation under different transmitter power levels

We conducted additional simulation rounds using the established simulation setup (Table 6), introducing variations in transmitter power to investigate its influence on key performance parameters (where RC is fixed and equal to 1). Specifically, we examined transmitter powers of 20 dBm (shown in blue in Figs. 21 to 25) and subsequently increased the power to 23 dBm (shown in red in Figs. 21 to 25). Our primary focus was to understand how increasing transmit power influences the behavior of key performance metrics.

In this analysis, we limited our exploration to three values of the persistence probability: the lower threshold at 0 (solid lines in Figs. 21 to 25), the upper threshold at 0.99 (dashed line in Figs. 21 to 25), and the optimal persistence probability identified in Section 5.5, set at 0.6 (represented by a dotted line in Figs. 21 to 25). Additional persistence probability values can be inferred by interpolation based on the findings in Section 5.5.

Fig. 21 displays the dependence of PDR on the distance between nodes. Across all the persistence probability values considered, we observed that higher transmitter power leads to inferior PDR performance when the node distance is less than 150 m, while showing improved performance beyond 150 m. This suggests that increasing transmit power may adversely affect the probability of successful packet transmission at shorter distances, especially for nodes in close proximity, where PDR is particularly demanding for safety reasons. This behavior of PDR is attributed to the fact that increasing transmit power not only mitigates the effects of signal attenuation, but also amplifies interference and potential collisions in the channel. Evidence supporting this can be found in Figs. 22 and 23. Fig. 22 depicts CLR as a function of node distance, revealing consistently higher CLR values when the transmitter power is 23 dBm. Meanwhile, Fig. 23 compares PLR as a function of node distance, showing the expected reduction in losses due to signal attenuation when a more powerful transmitter is employed.

Fig. 24 illustrates the relationship between PAoI and distance, which is consistent with the findings in Fig. 14. Notably, despite the lower PDR at distances below 150 m with higher transmit power, PAoI does not exhibit a corresponding decline. Higher transmit power allows for

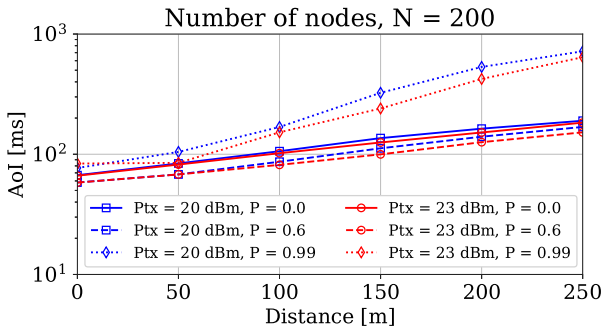

Fig. 25. AoI as a function of distance (log-scale). (For interpretation of the references to color in this figure legend, the reader is referred to the web version of this article.)

lower PAoI values at all persistence probability settings, highlighting its effectiveness in achieving improved outcomes.

A similar trend can be seen in Fig. 25, which plots the AoI on a logarithmic scale. However, optimal performance is observed when a persistence probability of 0.6 is used for both transmitter powers. This underscores the non-monotonic nature of the AoI with respect to the persistence probability, which emphasizes the existence of an optimal value.

6. Conclusion

This paper presents a thorough analysis of medium access control in 5G NR-V2X sidelink communications. The study employs a variety of methodologies, including analytical modeling and simulations in both a simplified MATLAB-based setting and a widely-used realistic ns-3 environment. It includes a simplified analytical model that examines the relationship between the persistence probability of SPS and the AoI. The paper also proposes an extension to the model to capture the effect of distance-based propagation and fading. Simulation results demonstrate the existence of an optimal level that minimizes the AoI. Additionally, the paper provides insight into the complex interaction of different system parameters and channel characteristics, identifying limitations of the SPS mechanism and suggesting the need for further improvements.

Future work will investigate the effect of spatial re-use of radio resources over a long highway, extend the simulation model to urban scenarios with more realistic mobility models, and extend the stochastic geometry model to include the effect of sensing.

CRediT authorship contribution statement

Alexey Rolich: Writing – review & editing, Writing – original draft, Visualization, Validation, Software, Conceptualization. **Ion Turcanu:** Writing – review & editing, Writing – original draft, Conceptualization. **Alexey Vinel:** Writing – review & editing. **Andrea Baiocchi:** Writing – review & editing, Writing – original draft, Visualization, Validation, Supervision, Project administration, Methodology, Formal analysis, Conceptualization.

Data availability

No data was used for the research described in the article.

Acknowledgments

This work has been partially supported by the Luxembourg National Research Fund (FNR) under the project CANDI (INTER/ANR/22/17192457). This work was partially supported by the Sapienza University of Rome, Italy under the grant n. RP123188F68315A5, project title "Modeling and optimization of sidelink communications in C-V2X 5G NR". This work has also been partially supported by the Ministry of University and Research of Italy, under the PRIN program, project code: 20223Y85JN, project title: "LOREN - LOw-delay congestion control for REal-time applications over the iNternet".

Appendix. Proof of Theorem 1

The fixed point iteration in Eq. (10) can be re-written with reference to the variable $x = q/\overline{K}_e$. Since $\overline{K}_e$ ranges between $K - N$ and $K - 1$ (since at least one SC is busy), it must be $x \in [q/(K-1), q/(K-N)]$. Moreover, it must be $K \geq 2$ (otherwise there is no alternative for selection) and $N \geq K - 1$ (by hypothesis of the Theorem).

Using the mean field approximation, we have $x = q/(K\tilde{\pi}_0)$. Then, the fixed point iteration can be written as follows:

$$x = \frac{q}{K}\left(1 + \mathbf{v}(x)\mathbf{z}\right) = \phi(x) \tag{A.1}$$

where $\mathbf{z} = (\mathbf{I} - \mathbf{A})^{-1}\mathbf{e}$ is a non-negative column vector, $\mathbf{e}$ is a column vector of 1's, and $\mathbf{v} = [P(0,1), \ldots, P(0,N)]$, with $P(0,k) = \binom{N}{k}x^k(1-x)^{N-k}$ for $k = 1, \ldots, N$. In Eq. (A.1) we have emphasized the dependence of the components of vector $\mathbf{v}$ on x and have introduced the function $\phi(x)$.

The fixed point equation $x = \phi(x)$ is to be considered for $x \in [q/(K-1), q/(K-N)]$. We prove that a unique positive solution of the fixed point equation exists in this interval for $K \geq 2$ and $1 \leq N \leq K-1$.

For that purpose, we note that it must be $q > 0$ (otherwise nodes would stick to their initially selected SC forever). Then, we exploit the special structure of the matrix $\mathbf{A}$, namely the fact that for $n = 1, \ldots, N$ it is $A_{n,k} = \binom{n}{k}(1-q)^k q^{n-k}$, for $k = 1, \ldots, n$ and $A_{n,k} = 0$ for $k = n+1, \ldots, N$. After some calculations, it is found that

$$\mathbf{v}(x)\mathbf{A} = \mathbf{v}\left(x(1-q)\right) \tag{A.2}$$

By repeating r times the application of Eq. (A.2), we get

$$\mathbf{v}(x)\mathbf{A}^r = \mathbf{v}\left(x(1-q)^r\right) \tag{A.3}$$

for $r \geq 0$. Using the series expansion of $(\mathbf{I} - \mathbf{A})^{-1}$, we have

$$\begin{aligned}\mathbf{v}(x)\mathbf{z} &= \mathbf{v}(x)(\mathbf{I} - \mathbf{A})^{-1}\mathbf{e} \\ &= \sum_{r=0}^{\infty}\mathbf{v}(x)\mathbf{A}^r\mathbf{e} = \sum_{r=0}^{\infty}\mathbf{v}\left(x(1-q)^r\right)\mathbf{e}\end{aligned}$$

Given the structure of the vector $\mathbf{v} = [P(0,1), \ldots, P(0,N)]$, with $P(0,k) = \binom{N}{k}x^k(1-x)^{N-k}$ for $k = 1, \ldots, N$, it is easy to see that $\mathbf{v}(x)\mathbf{e} = P(0,1) + \cdots + P(0,N) = 1 - P(0,0) = 1 - (1-x)^N$. Therefore, we get finally

$$\phi(x) = \frac{q}{K}\left[1 + \sum_{r=0}^{\infty}\left[1 - \left(1 - x(1-q)^r\right)^N\right]\right] \tag{A.4}$$

The series in Eq. (A.4) is absolutely convergent, hence it can be derived term by term, obtaining:

$$\phi'(x) = \frac{qN}{K}\sum_{r=0}^{\infty}(1-q)^r\left(1 - x(1-q)^r\right)^{N-1} \tag{A.5}$$

Since $\left(1 - x(1-q)^r\right)^{N-1}$ is positive and less than 1 for any $x, q \in (0,1)$ and any $N \geq 1$, we have

$$0 < \phi'(x) < \frac{qN}{K}\sum_{r=0}^{\infty}(1-q)^r = \frac{N}{K} < 1 \tag{A.6}$$

where the last inequality stems from the assumption $N < K$. This proves that $\phi(x)$ is monotonously strictly increasing in $[q/(K-1), q/(K-N)]$.

To complete the proof of existence and uniqueness of a solution to $x = \phi(x)$ in the considered interval, it suffices to show that

$$\phi\left(\frac{q}{K-1}\right) > \frac{q}{K-1} \tag{A.7}$$

$$\phi\left(\frac{q}{K-N}\right) \leq \frac{q}{K-N} \tag{A.8}$$

As for the first inequality, from Eq. (A.4) and $(1-x(1-q)^r)^N < 1-x(1-q)^r$, holding for all non-negative r, we get

$$\phi(x) > \frac{q}{K}\left[1+\sum_{r=0}^{\infty} x(1-q)^r\right] = \frac{q}{K}\left[1+\frac{x}{q}\right] \tag{A.9}$$

Then

$$\phi\left(\frac{q}{K-1}\right) > \frac{q}{K}\left[1+\frac{1}{q}\frac{q}{K-1}\right] = \frac{q}{K}\frac{K}{K-1} = \frac{q}{K-1} \tag{A.10}$$

As for the second inequality, let $\mathbf{u} = [1\ 2\ 3\ \ldots\ N]^{\mathrm{T}}$. It can be verified that $\mathbf{u}$ is the right eigenvector of $\mathbf{A}$ corresponding to the dominant eigenvalue $1-q$, i.e., $\mathbf{A}\mathbf{u} = (1-q)\mathbf{u}$. Then, we have $(\mathbf{I}-\mathbf{A})^{-1}\mathbf{u} = \frac{1}{q}\mathbf{u}$. The inverse of the matrix $\mathbf{I}-\mathbf{A}$ exists since $\mathbf{A}$ is strictly sub-stochastic. From the trivial inequality $\mathbf{e} \le \mathbf{u}$ and the non-negativity of entries of $(\mathbf{I}-\mathbf{A})^{-1}$, it is possible to derive that

$$\mathbf{z} = (\mathbf{I}-\mathbf{A})^{-1}\mathbf{e} \le (\mathbf{I}-\mathbf{A})^{-1}\mathbf{u} = \frac{1}{q}\mathbf{u} \tag{A.11}$$

Then

$$\phi(x) = \frac{q}{K}\left[1+\mathbf{v}(x)\mathbf{z}\right] \le \frac{q}{K}\left[1+\frac{1}{q}\mathbf{v}(x)\mathbf{u}\right] \tag{A.12}$$

Reminding the definitions of $\mathbf{v}(x)$ and $\mathbf{u}$, we have

$$\mathbf{v}(x)\mathbf{u} = \sum_{k=1}^{N}\binom{N}{k} k\, x^k (1-x)^{N-k} = Nx \tag{A.13}$$

Hence

$$\phi\left(\frac{q}{K-N}\right) \le \frac{q}{K}\left[1+\frac{1}{q}N\frac{q}{K-N}\right] = \frac{q}{K-N} \tag{A.14}$$

We have thus proved that the curve $y = \phi(x)$ is a strictly monotonously increasing function in $[q/(K-1), q/(K-N)]$, that is above the line $y = x$ at the left extreme of the interval, and it cannot be above $y = x$ at the right extreme. Hence, there must exists a unique intersection point ξ, belonging to the interior of the considered interval, or coinciding with its upper extreme.

Since the derivative of the iteration function is strictly less than 1 in the whole interval, the fixed point iteration is a contraction over the entire considered interval. Therefore, the sequence of approximations $x_{j+1} = \phi(x_j)$, $j \ge 0$, starting with $x_0 \in [q/(K-1), q/(K-N)]$ converges for any choice of the initial point belonging to the considered interval.

This completes the proof. □

References

[1] K. Hartman, K. Wunderlich, M. Vasudevan, K. Thompson, B. Staples, S. Asare, J. Chang, J. Anderson, A. Ali, et al., Advancing Interoperable Connectivity Deployment: Connected Vehicle Pilot Deployment Results and Findings, Tech. rep., United States. Department of Transportation. Intelligent Transportation Systems Joint Program Office, 2023.

[2] 5G-PPP, SNS JU Ecosystem, From R&I to Actual Deployment: Update on 5G Trials and Pilots for Connected and Automated Mobility, White paper, 6G Smart Networks and Services Industry Association, 2023.

[3] C. Viktorsson, V. Baid, C. Roberg, T. Geißler, M. Tarkiainen, Roadmap for Service Implementation Beyond Initial Deployment - Version 2021, Tech. rep., European ITS Platform, 2021.

[4] M. Torrent-Moreno, J. Mittag, P. Santi, H. Hartenstein, Vehicle-to-vehicle communication: Fair transmit power control for safety-critical information, IEEE Trans. Veh. Technol. 58 (7) (2009) 3684–3703, http://dx.doi.org/10.1109/TVT.2009.2017545.

[5] Q. Delooz, A. Willecke, K. Garlichs, A.-C. Hagau, L. Wolf, A. Vinel, A. Festag, Analysis and evaluation of information redundancy mitigation for v2x collective perception, IEEE Access 10 (2022) 47076–47093, http://dx.doi.org/10.1109/ACCESS.2022.3170029.

[6] A. Hegde, Q. Delooz, C.L. Mariyaklla, A. Festag, F. Klingler, Radio resource allocation for collective perception in 5G-NR vehicle-to-X communication systems, in: IEEE Wireless Communications and Networking Conference, WCNC, IEEE, 2023, pp. 1–7, http://dx.doi.org/10.1109/WCNC55385.2023.10118606.

[7] H.M. Wang, S.S. Avedisov, O. Altintas, G. Orosz, Multi-vehicle conflict management with status and intent sharing under time delays, IEEE Trans. Intell. Veh. (2022) http://dx.doi.org/10.1109/TIV.2022.3231639.

[8] G. Naik, B. Choudhury, J.-M. Park, IEEE 802.11 bd & 5G NR V2X: Evolution of radio access technologies for V2X communications, IEEE Access 7 (2019) 70169–70184, http://dx.doi.org/10.1109/ACCESS.2019.2919489.

[9] J.B. Kenney, Dedicated short-range communications (DSRC) standards in the United States, Proc. IEEE 99 (7) (2011) 1162–1182, http://dx.doi.org/10.1109/JPROC.2011.2132790.

[10] European Telecommunications Standards Institute, Intelligent Transport Systems (ITS); ITS-G5 Access Layer Specification for Intelligent Transport Systems Operating in the 5 GHz Frequency Band, EN 302 663 V1.3.1, ETSI, 2020.

[11] European Telecommunications Standards Institute, Intelligent Transport Systems (ITS); LTE-V2X Access Layer Specification for Intelligent Transport Systems Operating in the 5 GHz Frequency Band, EN 303 613 V1.1.1, ETSI, 2020.

[12] M. Harounabadi, D.M. Soleymani, S. Bhadauria, M. Leyh, E. Roth-Mandutz, V2X in 3GPP standardization: NR sidelink in release-16 and beyond, IEEE Commun. Stand. Mag. 5 (1) (2021) 12–21, http://dx.doi.org/10.1109/MCOMSTD.001.2000070.

[13] T.-K. Liu, J.A. Silvester, A. Polydoros, Performance evaluation of R-ALOHA in distributed packet radio networks with hard real-time communications, in: IEEE 45th Vehicular Technology Conference. Countdown To the Wireless Twenty-First Century, Vol. 2, IEEE, 1995, pp. 554–558, http://dx.doi.org/10.1109/VETEC.1995.504929.

[14] R.D. Yates, Y. Sun, D.R. Brown, S.K. Kaul, E. Modiano, S. Ulukus, Age of information: An introduction and survey, IEEE J. Sel. Areas Commun. 39 (5) (2021) 1183–1210, http://dx.doi.org/10.1109/JSAC.2021.3065072.

[15] Z. Chen, N. Pappas, E. Björnson, E.G. Larsson, Optimizing information freshness in a multiple access channel with heterogeneous devices, IEEE Open J. Commun. Soc. 2 (2021) 456–470, http://dx.doi.org/10.1109/OJCOMS.2021.3062678.

[16] A. Baiocchi, I. Turcanu, N. Lyamin, K. Sjoöberg, A. Vinel, Age of information in IEEE 802.11p, in: 17th IFIP/IEEE International Symposium on Integrated Network Management (IM): ITAVT Workshop, IEEE, Virtual Conference, 2021, pp. 1024–1031.

[17] J. Thunberg, D. Bischoff, F.A. Schiegg, T. Meuser, A. Vinel, Unreliable V2X communication in cooperative driving: Safety times for emergency braking, IEEE Access 9 (2021) 148024–148036, http://dx.doi.org/10.1109/ACCESS.2021.3124450.

[18] A. Rolich, I. Turcanu, A. Vinel, A. Baiocchi, Impact of persistence on the age of information in 5G NR-V2X sidelink communications, in: 21st Mediterranean Communication and Computer Networking Conference, MedComNet, IEEE, Ponza Island, Italy, 2023, pp. 15–24, http://dx.doi.org/10.1109/MedComNet58619.2023.10168874.

[19] European Telecommunications Standards Institute, Digital Cellular Telecommunications System (Phase 2+) (GSM) ; Universal Mobile Telecommunications System(UMTS) ; LTE ; 5G ; Release 16 Description; Summary of Rel-16 Work Items (3GPP TR 21.916 Version 16.2.0 Release 16), TR 121 916 V16.2.0, ETSI, 2022.

[20] M.H.C. Garcia, A. Molina-Galan, M. Boban, J. Gozalvez, B. Coll-Perales, T. Şahin, A. Kousaridas, A tutorial on 5G NR V2X communications, IEEE Commun. Surv. Tutor. 23 (3) (2021) 1972–2026, http://dx.doi.org/10.1109/COMST.2021.3057017.

[21] Z. Ali, S. Lagén, L. Giupponi, R. Rouil, 3GPP NR V2X mode 2: overview, models and system-level evaluation, IEEE Access 9 (2021) 89554–89579, http://dx.doi.org/10.1109/ACCESS.2021.3090855.

[22] T.T.T. Le, S. Moh, Comprehensive survey of radio resource allocation schemes for 5G V2X communications, IEEE Access 9 (2021) 123117–123133, http://dx.doi.org/10.1109/ACCESS.2021.3109894.

[23] K. Sehla, T.M.T. Nguyen, G. Pujolle, P.B. Velloso, Resource allocation modes in C-V2X: from LTE-V2X to 5G-V2X, IEEE Internet Things J. 9 (11) (2022) 8291–8314, http://dx.doi.org/10.1109/JIOT.2022.3159591.

[24] European Telecommunications Standards Institute, LTE; 5G; Overall Description of Radio Access Network (RAN) Aspects for Vehicle-To-Everything (V2X) Based on LTE and NR (3GPP TR 37.985 Version 17.1.1 Release 17), TR 137 985 V17.1.1, ETSI, 2022.

[25] European Telecommunications Standards Institute, 5G; NR; Radio Resource Control (RRC); Protocol Specification (3GPP TS 38.331 Version 17.3.0 Release 17), TS 138 331 V17.3.0, ETSI, 2023.

[26] M. Gonzalez-Martín, M. Sepulcre, R. Molina-Masegosa, J. Gozalvez, Analytical models of the performance of C-V2X mode 4 vehicular communications, IEEE Trans. Veh. Technol. 68 (2) (2018) 1155–1166, http://dx.doi.org/10.1109/TVT.2018.2888704.

[27] European Telecommunications Standards Institute, Digital Cellular Telecommunications System (Phase 2+) (GSM); Universal Mobile Telecommunications System (UMTS); LTE; 5G; Release Description; Release 14 (3GPP TR 21.914 Version 14.0.0 Release 14), TR 121 914 V14.0.0, ETSI, 2018.

[28] M. Segata, P. Arvani, R. Lo Cigno, A critical assessment of C-V2X resource allocation scheme for platooning applications, in: 16th Annual Conference on Wireless on-Demand Network Systems and Services Conference, WONS, IEEE, 2021, pp. 1–8, http://dx.doi.org/10.23919/WONS51326.2021.9415551.

[29] R. Molina-Masegosa, J. Gozalvez, M. Sepulcre, Configuration of the C-V2X mode 4 sidelink PC5 interface for vehicular communication, in: 2018 14th International Conference on Mobile Ad-Hoc and Sensor Networks, MSN, IEEE, 2018, pp. 43–48, http://dx.doi.org/10.1109/MSN.2018.00014.

[30] X. Gu, J. Peng, L. Cai, Y. Cheng, X. Zhang, W. Liu, Z. Huang, Performance analysis and optimization for semi-persistent scheduling in C-V2X, IEEE Trans. Veh. Technol. (2022) http://dx.doi.org/10.1109/TVT.2022.3223414.

[31] A. Bazzi, C. Campolo, A. Molinaro, A.O. Berthet, B.M. Masini, A. Zanella, On wireless blind spots in the C-V2X sidelink, IEEE Trans. Veh. Technol. 69 (8) (2020) 9239–9243, http://dx.doi.org/10.1109/TVT.2020.3001074.

[32] J. Wu, Y. Guo, S. Zhou, A reliable self-adaptive scheduling control protocol for cellular V2X mode 4, IEEE Access 10 (2022) 63991–64003, http://dx.doi.org/10.1109/ACCESS.2022.3183186.

[33] L. Lusvarghi, M.L. Merani, On the coexistence of aperiodic and periodic traffic in cellular vehicle-to-everything, IEEE Access 8 (2020) 207076–207088, http://dx.doi.org/10.1109/ACCESS.2020.3038307.

[34] S. Bartoletti, B.M. Masini, V. Martinez, I. Sarris, A. Bazzi, Impact of the generation interval on the performance of sidelink C-V2X autonomous mode, IEEE Access 9 (2021) 35121–35135, http://dx.doi.org/10.1109/ACCESS.2021.3061913.

[35] Y. Jeon, S. Kuk, H. Kim, Reducing message collisions in sensing-based semi-persistent scheduling (SPS) by using reselection lookaheads in cellular V2X, Sensors 18 (12) (2018) 4388, http://dx.doi.org/10.3390/s18124388.

[36] V. Todisco, S. Bartoletti, C. Campolo, A. Molinaro, A.O. Berthet, A. Bazzi, Performance analysis of sidelink 5G-V2X mode 2 through an open-source simulator, IEEE Access 9 (2021) 145648–145661, http://dx.doi.org/10.1109/ACCESS.2021.3121151.

[37] A. Molina-Galan, B. Coll-Perales, L. Lusvarghi, J. Gozalvez, M.L. Merani, How does 5G NR V2X mode 2 handle aperiodic packets and variable packet sizes? in: 2022 IEEE 23rd International Conference on High Performance Switching and Routing, HPSR, IEEE, 2022, pp. 183–188, http://dx.doi.org/10.1109/HPSR54439.2022.9831314.

[38] L. Cao, S. Roy, H. Yin, Resource allocation in 5G platoon communication: Modeling, analysis and optimization, IEEE Trans. Veh. Technol. 72 (4) (2022) 5035–5048, http://dx.doi.org/10.1109/TVT.2022.3223351.

[39] L. Lusvarghi, A. Molina-Galan, B. Coll-Perales, J. Gozalvez, M.L. Merani, A comparative analysis of the semi-persistent and dynamic scheduling schemes in NR-V2X mode 2, Veh. Commun. (2023) 100628, http://dx.doi.org/10.1016/j.vehcom.2023.100628.

[40] J. Yin, S.-H. Hwang, Reuse distance-aided resource selection mechanisms for NR-V2X sidelink communication, Sensors 24 (1) (2024) 253.

[41] L. Lusvarghi, M.L. Merani, Machine learning for disseminating cooperative awareness messages in cellular V2V communications, IEEE Trans. Veh. Technol. 71 (7) (2022) 7890–7903, http://dx.doi.org/10.1109/TVT.2022.3170982.

[42] S. Kuang, P. Wang, Y. Shen, Z. Li, Efficient resource allocation scheme for aperiodic traffic in NR V2X communications through adaptive reservation and selection, in: 8th International Conference on Communication, Image and Signal Processing, CCISP, IEEE, 2023, pp. 437–443, http://dx.doi.org/10.1109/CCISP59915.2023.10355839.

[43] A. Bazzi, C. Campolo, V. Todisco, S. Bartoletti, N. Decarli, A. Molinaro, A.O. Berthet, R.A. Stirling-Gallacher, Toward 6G vehicle-to-everything sidelink: Nonorthogonal multiple access in the autonomous mode, IEEE Veh. Technol. Mag. 18 (2) (2023) 50–59, http://dx.doi.org/10.1109/MVT.2023.3252278.

[44] V. Todisco, C. Campolo, A. Molinaro, A.O. Berthet, R.A. Stirling-Gallacher, A. Bazzi, Joint use of self and successive interference cancellation in V2X sidelink with autonomous resource allocation, in: IEEE 97th Vehicular Technology Conference, VTC2023-Spring, IEEE, 2023, pp. 1–7, http://dx.doi.org/10.1109/VTC2023-Spring57618.2023.10199403.

[45] G. Twardokus, H. Rahbari, Towards protecting 5G sidelink scheduling in C-V2X against intelligent DoS attacks, IEEE Trans. Wireless Commun. 22 (11) (2023) 7273–7286, http://dx.doi.org/10.1109/TWC.2023.3249665.

[46] S. Kaul, M. Gruteser, V. Rai, J. Kenney, Minimizing age of information in vehicular networks, in: 8th Annual IEEE Communications Society Conference on Sensor, Mesh and Ad Hoc Communications and Networks, 2011, pp. 350–358, http://dx.doi.org/10.1109/SAHCN.2011.5984917.

[47] D. Plöger, M. Segata, R. Lo Cigno, A. Timm-Giel, Markov-modulated models to estimate the age of information in cooperative driving, in: IEEE Vehicular Networking Conference, VNC, 2019, pp. 1–4, http://dx.doi.org/10.1109/VNC48660.2019.9062802.

[48] I. Turcanu, A. Baiocchi, N. Lyamin, A. Vinel, An age-of-information perspective on decentralized congestion control in vehicular networks, in: 19th Mediterranean Communication and Computer Networking Conference, MedComNet, IEEE, ISBN: 978-1-6654-1177-6, 2021, pp. 1–8, http://dx.doi.org/10.1109/MedComNet52149.2021.9501273.

[49] F. Peng, Z. Jiang, S. Zhang, S. Xu, Age of information optimized MAC in V2X sidelink via piggyback-based collaboration, IEEE Trans. Wireless Commun. 20 (1) (2020) 607–622, http://dx.doi.org/10.1109/TWC.2020.3027353.

[50] A. Dayal, V.K. Shah, H.S. Dhillon, J.H. Reed, Adaptive RRI selection algorithms for improved cooperative awareness in decentralized NR-V2X, IEEE Access 11 (2023) 134575–134588, http://dx.doi.org/10.1109/ACCESS.2023.3336686.

[51] A. Fouda, R. Berry, I. Vukovic, Interleaved one-shot semi-persistent scheduling for BSM transmissions in C-V2X networks, in: IEEE Vehicular Networking Conference, VNC, 2021, pp. 143–150, http://dx.doi.org/10.1109/VNC52810.2021.9644679.

[52] M.M. Saad, M.A. Tariq, J. Seo, M. Ajmal, D. Kim, Age-of-information aware intelligent MAC for congestion control in NR-V2X, in: 14th International Conference on Ubiquitous and Future Networks, ICUFN, IEEE, 2023, pp. 265–270, http://dx.doi.org/10.1109/ICUFN57995.2023.10200859.

[53] L. Cao, H. Yin, R. Wei, L. Zhang, Optimize semi-persistent scheduling in NR-V2X: An age-of-information perspective, in: 2022 IEEE Wireless Communications and Networking Conference, WCNC, 2022, pp. 2053–2058, http://dx.doi.org/10.1109/WCNC51071.2022.9771765.

[54] Z. Mlika, S. Cherkaoui, Deep deterministic policy gradient to minimize the age of information in cellular V2X communications, IEEE Trans. Intell. Transp. Syst. 23 (12) (2022) 23597–23612, http://dx.doi.org/10.1109/TITS.2022.3190799.

[55] M. Haenggi, Stochastic Geometry for Wireless Networks, Cambridge University Press, 2012.

[56] NSNAM, ns-3 Network Simulator, 2024, https://github.com/nsnam.

[57] L. Lusvarghi, M.L. Merani, MoReV2X - A new radio vehicular communication module for ns-3, in: 2021 IEEE 94th Vehicular Technology Conference, VTC2021-Fall, 2021, pp. 1–7, http://dx.doi.org/10.1109/VTC2021-Fall52928.2021.9625478.

[58] L. Lusvarghi, MoReV2X, 2024, https://github.com/LLusvarghi/MoReV2X.

[59] 3GPP, Study on Evaluation Methodology of New Vehicle-To-Everything (V2X) Use Cases for LTE and NR;(Release 15), TR 37.885 V15.3.0, 3GPP, 2019.

[60] European Telecommunications Standards Institute, Intelligent Transport Systems (ITS). Study on Receiver Requirements in ETSI EN 302 571, TR 103 688 V1.1.1, ETSI, 2022.

[61] European Telecommunications Standards Institute, 5G; NR; Physical Layer Procedures for Data (3GPP TS 38.214 Version 17.1.0 Release 17), TS 138 214 V17.1.0, ETSI, 2022.

[62] European Telecommunications Standards Institute, 5G; NR; Physical Layer Measurements (3GPP TS 38.215 Version 17.1.0 Release 17), TS 138 215 V17.1.0, ETSI, 2022.

[63] H. Huawei, R1-1900852 Link Level Evaluations on Sidelink for NR V2X, Ad Hoc Meeting 1901, 3GPP TSG RAN WG1, 2019.

[64] Ericsson, R1-1903180, Link Level Evaluations of NR PSCCH, Meeting 96, 3GPP TSG-RAN WG1, 2019.

Alexey Rolich is Ph.D. Student in Department of Information Engineering, Electronics and Telecommunications at the University of Rome La Sapienza. He gained bachelor's and master's degrees at National Research University Higher School of Economics in Moscow, Russia. Research interests are focused on vehicular networks, medium access control protocols, cellular radio networks, simulations and performance evaluation. Alexey Rolich is the author of more than 20 publications in international journals and conference proceedings, and recipient of Mario Gerla Best Paper Award at the 21st Mediterranean Communication and Computer Networking Conference (MedComNet 2023).

Ion Turcanu is a Senior Researcher and Head of the Edge Computing and Networks Group at the Luxembourg Institute of Science and Technology (LIST). He joined LIST in 2021 after having spent four years as a postdoctoral researcher at the Interdisciplinary Centre for Security, Reliability and Trust, University of Luxembourg. His research expertise is in the areas of next-generation mobile networks, cooperative networked systems, V2X communications, connected and automated mobility, and time-sensitive networking. He has over 30 peer-reviewed publications in prestigious venues with over 350 citations. He received the "Mario Gerla Best Paper Award" from the 21st Mediterranean Communication and Computer Networking Conference (MedComNet 2023). He has served as a reviewer for several reputable journals, including IEEE Transaction on Mobile Computing, IEEE Transactions on Vehicular Technology, and IEEE Communications Magazine. He has also served on the technical and executive committees of several conferences including TPC Co-Chair for MedComNet 2024, TPC Track Chair for IEEE MELECON 2022, and TPC Member for IEEE CCNC (2019-onwards) and IEEE WCNC (2022–2023).

Alexey Vinel is a professor at the Karlsruhe Institute of Technology (KIT), Germany. Before he joined KIT in October 2022, he was a professor at the University of Passau, Germany. Since 2015, he has been a professor at Halmstad University, Sweden (now part-time). His research interests include vehicular communications and cooperative autonomous driving. He has led several research projects including the Knowledge Foundation synergy project SafeSmart 2019–2024. He received his Ph.D. degree from the Tampere University of Technology, Finland, in 2013. He has been a recipient of Alexander von Humboldt Foundation fellowship in 2008.

Andrea Baiocchi received his "Laurea" degree in Electronics Engineering in 1987 and his Ph.D. degree in Information and Communications Engineering in 1992, both from the University of Roma "La Sapienza". Since January 2005 he is a Full Professor in the Department of Information Engineering, Electronics and Telecommunications of the University of Roma Sapienza. His main scientific contributions are on telecommunications network traffic engineering, queuing theory, resource sharing and congestion control. His current research interests focus on massive multiple access and vehicular networking. Andrea's research activities have been carried out also in the framework of many national (CNR, MIUR, POR) and international (European Union, ESA) projects, also taking coordination and responsibility roles. Andrea has published more than 170 papers on international journals and conference proceedings. He has participated to the Technical Program Committees of eighty international conferences. He also served in the editorial board of the telecommunications technical journal published by Telecom Italia (currently TIM) for ten years. He is currently Associate Editor of Elsevier Vehicular Communications journal. He is the author of the book "Network Traffic Engineering – Stochastic models and Applications", Wiley, 2020.